The multicomponent exchange of metals between magmatic fluids and silicate melts

Austin M Gion, Fabrice Gaillard

Journal Pre-proofs

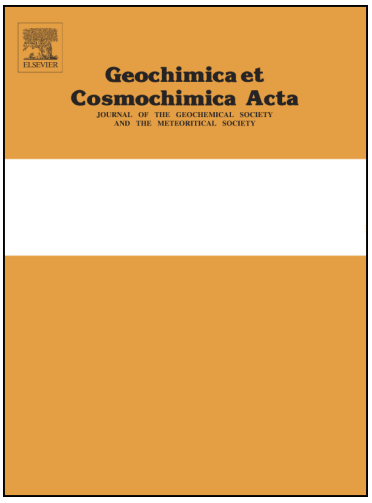

The multicomponent exchange of metals between magmatic fluids and silicate melts

Austin M. Gion, Fabrice Gaillard

PII: S0016-7037(25)00043-2
DOI: https://doi.org/10.1016/j.gca.2025.01.033
Reference: GCA 13717

To appear in: *Geochimica et Cosmochimica Acta*

Received Date: 29 July 2024
Accepted Date: 23 January 2025

Please cite this article as: Gion, A.M., Gaillard, F., The multicomponent exchange of metals between magmatic fluids and silicate melts, *Geochimica et Cosmochimica Acta* (2025), doi: https://doi.org/10.1016/j.gca.2025.01.033

The Multicomponent Exchange of Metals Between Magmatic Fluids and Silicate Melts

Austin M. Gion[1,2*] and Fabrice Gaillard[1]

[1]Univ. Orléans, CNRS, BRGM, ISTO, UMR 7327, 1A Rue de la Férollerie – CS 20066, 45071 Orléans Cedex 2, France

[2] Department of Earth Science, University of Oxford, South Parks Road, Oxford OX2 8NP, United Kingdom

*Author for correspondence (austin.gion@earth.ox.ac.uk; ORCID: 0000-0001-9124-039X).
†Present Address: Department of Earth Science, University of Oxford, South Parks Road, Oxford OX2 8NP, United Kingdom

Abstract

Magmatic fluids are an integral part of volcanic eruptions and the transport of metals through the crust. In order to understand this transport and the evolution of magmatic fluids, we performed experiments on rhyolitic melts saturated with an aqueous fluid at 800°C and 200 MPa and measured the major and trace element composition, as well as the chlorine and fluorine content in coexisting fluids and melts. We find that most trace elements are largely fluid immobile, i.e. partition coefficients of <1, with the exception of some transition metals, such as Cr, Ni, Cu, and Zn. Fluid mobility is primarily affected by the chlorine concentration of the fluid where increasing chlorine concentration in the fluid increases metal mobility. Such experimental observations have been previously parameterized using empirical relationships between partition coefficients and fluid salinity; however, such relationships do not consider metal speciation or fully capture the fluid-melt exchanges in which cations (major and trace elements) compete for available ligands (Cl, F, OH, etc.). In order to better characterize the behavior of metal in magmatic fluids we utilize existing thermodynamic databases and experimental fluid compositions to calculate the equilibrium concentration of aqueous hydroxide, chloride, and fluoride species in the fluid phase. The equilibrium concentrations of each species were then used to calculate apparent equilibrium constants and characterize the exchange of 42 cations between the fluid and silicate melts for 129 aqueous species. We find that these apparent equilibrium constants vary as a function of the HCl and HF content of the experimental fluid. We further present a model based on these experimentally determined apparent equilibrium constants that is capable of calculating fluid-melt equilibria. This model can subsequently be used to predict fluid-melt partition coefficients for metals, as well as chlorine and fluorine, over a wide range of P-T-X conditions.

Keywords: magmatic-hydrothermal, multicomponent fluids, metal exchange, equilibrium constant, numerical modelling

1. Introduction

Magmatic fluids are H_2O-rich and contain variable concentrations of CO_2 and S, halogens, and metals (Hedenquist and Lowenstern, 1994; Černý et al., 2005; Guo and Audétat, 2017; Audétat, 2019; Webster et al., 2020; Tattitch et al., 2021). Such fluids form when silicate melts either decompress or undergo extensive crystallization, such that the melt reaches volatile saturation (Candela, 1997; Candela and Piccoli, 2005) and a fluid phase, which is either a supercritical fluid, a low-salinity vapor, or high-salinity brine (Bodnar et al., 1985; Richards, 2011) exsolves. These magmatic fluids ascend due to their relatively lower density and transport metals, which may be outgassed at the tops of volcanoes (Edmonds et al., 2022) or precipitate as ore-minerals at shallow depths (Hedenquist and Lowenstern, 1994). In order to understand the transportation of metals by magmatic fluids, it is vital to understand the behavior of metals in magmatic-hydrothermal systems. Nernst-type partition coefficients $\left(\mathrm{D_i^{Fluid/Melt}} = \mathrm{C_i^{Fluid}}/\mathrm{C_i^{Melt}}; C = \text{concentration of element i}\right)$ are a popular metric used to characterize the behavior of metals in magmatic-hydrothermal systems and allow for the direct use of experimental data. Many $\mathrm{D_i^{Fluid/Melt}}$ correlate with the salinity of fluids and this relationship has been widely used to predict metal behavior (Zajacz et al., 2008; Iveson et al., 2019). However, such a relationship cannot be generally used as a predictive tool, because it does not consider metal speciation or fully capture the fluid-melt exchanges in which cations (major and trace elements) compete for available ligands (Cl, F, OH, etc.) (Candela and Piccoli, 1998; Frank et al., 2003). Development of a multicomponent model is further complicated by the lack of thermodynamic data available and thus, a complete fluid-melt model has not previously been developed for metals in magmatic-hydrothermal systems.

At present, the thermodynamically rigorous models that do exist primarily focus on the solubility of water and carbon in silicate melts in addition to the speciation of hydrogen, oxygen, and carbon (Stolper, 1982; Papale et al., 2006; Iacovino et al., 2021; Gaillard et al., 2022; Papale et al., 2022), the solubility of chlorine (Thomas and Wood, 2023), or melt thermochemistry and redox state (Moretti and Ottonello, 2022). One of the most widely used thermodynamic models for understanding the evolution of silicate melts is the MELTS family of software (Ghiorso and Sack, 1995; Gualda et al., 2012; Ghiorso and Gualda, 2015; Antoshechkina and Ghiorso, 2018), which incorporates a H_2O and CO_2 solubility model and calculates the solubility of various mineral phases. In addition to these melt-focused models, there are a number of models that consider the speciation of metals in aqueous fluids. These models include DEW (Sverjensky et al., 2014) and SUPCRT (Johnson et al., 1992; Zimmer et al., 2016), which focus on calculating the thermodynamic properties of solutes and water in aqueous phases, as well as the equilibrium constants for reactions between minerals, gases, water and aqueous species. There are also a variety of programs that utilize similar databases as those employed by DEW and SUPCRT to model fluid-rock interactions, such as GEMS (Kulik et al., 2013), Geochemists Workbench (Bethke, 2007), PHREEQC (Parkhurst and Appelo, 2013), PFlotran (Hammond et al., 2019), and ToughReact (Sonnenthal et al., 2021). However, none of the above models are able to connect the metal content of magmatic fluids to the silicate melt. In the current work we present a thermodynamically rigorous model that bridges this knowledge gap and links magmatic fluids to silicate melts for both major and trace elements. This model is based on novel experiments that characterize the exchange of metals between fluids and silicate melts and is capable of describing the behavior of metals in magmatic-hydrothermal systems across a variety of melt compositions ranging from andesitic to rhyolitic to phonolitic at crustal pressure and temperature conditions. This model can be used to both identify knowledge gaps in thermodynamic databases for solutes in aqueous phases, as well as predict the degassing behavior of metals exsolving from silicate melts.

2. Experimental Methods

In order to better characterize the exchange of metals between fluids and silicate melts, we performed experiments in rhyolitic systems at a temperature of 800°C and a pressure of 200 MPa. The starting materials were powdered Macusani Rhyolite (glass with minor andalusite) (Pichavant et al., 1987; Pichavant et al., 1988), provided by Michel Pichavant; and the Bishop Tuff (B-628C; fused into a glass at 1400°C with relict quartz) (Hildreth, 1979), provided by Bruno Scaillet. These glasses were chosen as they are well studied and well constrained systems that correspond to either a near eutectic metaluminous melt (Bishop Tuff) or a peraluminous fluorinated melt (Macusani). Such compositions are relatively simple and are an ideal starting point for a new approach to fluid-melt studies. The composition of both starting glasses is given in Table 1. In addition to the starting glasses, one of five starting aqueous chloride solutions was used in each experimental charge. Aqueous chloride solutions were up to ~11 wt.% NaCl equiv. with NaCl:KCl ratio of 1:1 ± minor amounts of HCl (Table 2). NaCl and KCl were chosen as salts as they are the primary salts in magmatic-hydrothermal systems in the upper crust (Tattitch et al., 2021). A ratio of 1:1 was initially chosen as the Na:K ratio in the Bishop Tuff, on a mole basis, is near 1:1; although, the Na:K ratio of Macusani is 1.67:1 the 1:1 was maintained for consistency among experiments. The fluid/glass ratio of the experimental charges ranged from 0.2 to 1.1 in order to evaluate if fluid to melt ratio was a controlling parameter. All experiments also contained a 1.5 mm by 5 mm cuboid of inclusion-free synthetic quartz to help buffer the activity of SiO_2, which partially dissolved (mass change of ~4 relative %) in the fluid phase at the experimental conditions. In two Bishop Tuff experiments, variable amounts of fluorine was added as NaF, KF, and AlF_3 in a 1:1:2 ratio, which was chosen to maintain an ASI (aluminum saturation index defined as $Al_2O_3/(Na_2O + K_2O + (CaO - 3.33P_2O_5))$ on a molar basis) of the Bishop Tuff (ASI = ~1). The mass ratio of melt to fluorine-mix varied from 11 to 18, resulting in variable fluorine contents (Table 3). Additionally, in experiments where the fluorine mix was included, amorphous SiO_2 was added to prevent the melt from becoming overly enriched in alkalis (Table 3).

Experimental charges were contained in annealed gold capsules (5 mm outer diameter, ~20 mm length, and 0.2 mm wall thickness) that were cleaned in sequential baths of boiling, diluted HCl and boiling demineralized water. Starting materials were loaded into the capsules that were tri-crimped and welded on one end in the order of glass, aqueous solution ± fluoride salts, and the quartz cuboid, the latter of which was contained in an open 2 mm outer diameter capsule. Capsules were tri-crimped and welded closed and placed in a drying oven at 120°C overnight to check for leaks. Capsules exhibiting a weight loss (>1 mg) were discarded. The weights of the starting materials and the initial fluid/melt ratio of all experiments are given in Table 3.

Experiments were performed in an internally-heated pressure vessel (IHPV) or in a cold-seal pressure vessel (CSPV) at the Institut des Sciences de la Terre d'Orléans (ISTO), France. IHPV experiments were performed in the Clermont, Gros Bleu, and Gros Vert vessels at ISTO for a duration of 116 to 263 hours in the vertical position and contained up to 5 capsules + 1 oxygen fugacity (f_{O_2}) sensor. Each capsule contained either Macusani or Bishop Tuff and one of the five starting solutions. The IHPVs were fitted with either molybdenum, molybdenum-lanthanum, or Kanthal heating elements and temperature is continuously monitored by two type-S or type-K thermocouples located above and below the capsules. The pressure medium in IHPV experiments is a mixture of pure argon and 98%Ar - 2%H_2 (hydrogen is 2 vol%). The vessels were first pressurized with the 98%Ar - 2%H_2 mixture (~30 MPa) followed by pure argon (to 130-140 MPa). The target pressure is achieved upon heating and was continuously monitored by a transducer. The addition of hydrogen to the pressure medium allows f_{O_2} to be buffered during the experiment (Scaillet et al., 1992; Scaillet et al., 1995). Oxygen fugacity was buffered to ΔFMQ (fayalite-magnetite-quartz) ± 0.5 (Table 3) and monitored by using CoPd f_{O_2} sensors (Taylor et al., 1992) comprising a cobalt-palladium pellet (initial X_{Co} of 0.35), excess CoO, water, and a jacket of ZrO_2 powder contained within a gold capsule (3 mm outer diameter, 10 mm length, and 0.2 mm wall thickness). The IHPV experiments were quenched by turning off the power to the furnace and cooled by circulating water around the vessel. In one experiment (2 capsules), a drop quench was performed. For this drop quench, the experiment was initially quenched by turning off the vessel. The capsules were then removed from the vessel and the vessel was fitted with the drop-quench mechanism, which was an alumina crucible suspended by a platinum wire. The capsules were then reloaded and brought to run conditions for 1 hour before an electric current was passed through the platinum wire causing it to break and the alumina crucible to fall to the cold end of the vessel. The glass transition temperature was reached in less than seven minutes after turning off the IHPV and less than several seconds when quenching by turning off the power to the furnace and by drop quench, respectively.

The CSPV experiments were performed in nickel-based Inconel vessels for a duration of 450 to 644 hours. Each experiment contained two capsules (3mm outer diameter, 15-20 mm length. 0.2mm wall thickness), one with Bishop Tuff and one with the Macusani Rhyolite. Both capsules contained solution 4 (Table 2) and a quartz cuboid. Furnaces were kept in a sub-horizontal (angle of ~10°) position and vessels were externally heated by Kanthal furnace. The portion of the vessel that remained outside of the furnace was continuously water cooled. Temperature was monitored by a type-K thermocouple placed within a well at the end of the vessel near the experimental charge. The pressure medium was water, and the pressure was monitored by a Heise bourdon tube gauge. The f_{O_2} of the experiments was buffered by the intrinsic f_{O_2} of the vessel, which for nickel-based vessels is approximately Nickel-Nickel Oxide (NNO) + 1 (e.g. Tattitch et al., 2015; Gion et al., 2018). Experiments were quenched by removing the vessel from the furnace and allowing the vessel to be cooled by the circulating water. The glass reached the glass transition temperature in less than a few minutes.

3. Analytical Methods

3.1. Recovered Fluids

The recovery of run products and analytical methods, for both solutions and glasses, utilized in this study are discussed in detail in Gion et al. (2022) and follow a similar of that described by Iveson et al. (2019). For complete details the reader is referred to those studies. In brief, capsules were cleaned, submerged in deionized water, opened, and agitated to release the experimental fluid. Capsules were left submerged for a minimum of one week to equilibrate and the water was sampled. The length of time for diffusive equilibration occur between the water and the run product solution is based on the study of Iveson et al. (2019), who submerged capsules for a minimum of one week. After submerging capsules were dried and bathed in warm (~60°C) 5M HCl to dissolve any remaining precipitates for ~20 mins and repeat baths were performed when required. The deionized water and HCl bath were then combined, dried down, and recovered in nitric acid. Fluids were analyzed for major cations (Na^+, K^+,Ca^{2+}, and Mg^{2+}) and anions (F^- and Cl^-) by ion chromatography (IC) by using a ThermoFisher Dionex ICS-6000 instrument and for trace elements (Li, Be, Al, Si, Sc, Cr, V, Mn, Fe, Co, Ni, Cu, Zn, Ga, Ge, Rb, Sr, Y, La, Ce, Pr, Nd, Sm, Eu, Gd, Tb, Dy, Ho, Er, Tm, Yb, Lu, Zr, Nb, Mo, Cd, Sb, Ba, Hf, Pb, Th, and U) by inductively coupled plasma mass spectrometry (ICP-MS) by using a ThermoFisher Element-XR ICP-MS. The concentration of boron in the run product solutions was estimated by mass balance by using the method of Gion et al. (2022). Reproducibility of IC analyses and solution ICP-MS was determined by repeat measurements of external standards and was between 3 and 8 relative percent for IC analyses and ~10 relative percent for ICP-MS.

3.2. Glasses

Run product glasses were analyzed for Si, P, Ti, Al, Fe, Mg, Mn, Ca, Na, K, Cl, and F by wavelength dispersive spectroscopy by using a Cameca SX-Five electron probe micro analyzer (EPMA) with beam conditions of an accelerating voltage of 15 kV, a current of 5 nA, and a beam diameter of 20 µm. Analytical standards were albite, topaz, andradite, apatite, orthoclase, vanadinite, $MnTiO_3$, Fe_2O_3, and MgO.

The water content of the run product glasses was calculated by using a calibrated “by difference” method. The “by difference” method was calibrated by analyzing four rhyolite glass standards with variable water contents prior to and after all analyses as unknowns. The glass standards have the same major element composition (Table 1 of Scaillet and Evans (1999)) but are anhydrous or contain 2.42, 4.24, and 6.38 wt.% water, which was previously determined by Karl Fischer titration (Scaillet and Evans, 1999). A linear regression of the known water content vs the analytical total was then performed and yielded the equation wt.% H_2O = -0.82(analytical total) + 81.4. The concentration of Li_2O and B_2O_3 measured by LA-ICP-MS were also included in the analytical total because its exclusion resulted in a clear overestimation of the water content for Macusani glasses where Li_2O + B_2O_3 is ~1 wt.%. These rhyolite standards were also used to monitor diffusion of alkalis away from the election beam and reproducibility of the analyses. At the analytical conditions used here alkali diffusion away from beam is negligible. Additionally, across five analytical sessions the average glass compositions, normalized on an anhydrous basis, are within one standard deviation of the published compositions except for aluminum and potassium, which are within two standard deviations of published compositions.

The concentration of trace elements (Li, Be, B, Sc, V, Cr, Co, Ni, Cu, Zn, Ga, Ge, Rb, Sr, Y, Nb, Mo, Cd, In, Sn, Cs, Ba, La, Ce, Pr, Nd, Sm, Eu, Gd, Tb, Dy, Ho, Er, Tm, Yb, Lu, Ta, W, Au, Pb, Th, and U) in the run product glasses was measured by laser ablation inductively coupled mass spectrometry (LA-ICP-MS) by using a RESOlution-SE 193 nm Ar-F excimer laser with a S155 Laurin Technic sample cell coupled to a triple quadrupole Agilent 8900. Silicon was used as the internal standard and NIST610 was used as the external standard. Additionally, NIST612, BCR-2G, and BHVO-2G were analyzed as unknowns to monitor the accuracy of the analyses, which were within the accepted values with a bias of less than 10 relative percent. Data reduction was performed using the program SILLS (https://mineralsystems.ethz.ch/software/sills.html) (Guillong et al., 2008).

3.3. Uncertainties

Uncertainties in EPMA and LA-ICP-MS analyses are given in the supplementary tables as the standard deviations of the mean: $\sigma_m = \frac{\left(\sqrt{\frac{1}{n-1}\sum_{i=1}^{n}(x-\bar{x})^2}\right)}{\sqrt{n}}$ and all individual analyses are provided in the supplementary files. Uncertainties for solution ICP-MS and IC analyses are determined from the reproducibility of external standards.

4. Theoretical Framework

4.1. Fluid Speciation: Assumptions and Limitations

In order to step beyond Nernst-type partition coefficients, it is necessary to consider the speciation of metals in supercritical fluids. However, direct measurements of the fluid species present are not possible with the experimental techniques used in this study. This limitation necessitates the simplification of fluid speciation and the reliance on existing thermodynamic databases. We calculate the equilibrium concentration and Debye-Hükel activity coefficients for metals present as hydroxide, chloride, and fluoride species in the experimental fluids by using a mass balance and law of mass action approach modified after the equations of Crerar (1975). The equations used in this study, as well as a list of species considered, are provided in Table 4. Thermodynamic data are taken from SUPCRTBL (Johnson et al., 1992; Zimmer et al., 2016) and MINES19 (Gysi et al., 2023). These data sources are compilations of numerous thermodynamic studies conducted over a wide range of pressure and temperature conditions including the conditions at which the experiments in this work were performed. The internally consistent set of species that have been considered were chosen on the basis of four conditions. First, the species are either the dominant species for their respective metal-ligand pairs at the conditions of interest, i.e. NaCl, KCl, $CaCl_2$, $CuCl^-$, or analogous metal-ligand pairs for similar charged elements at relevant oxidation states (Kouzmanov et al., 2012; Pokrovski et al., 2013; Tattitch and Blundy, 2017) and contain only one metal and one ligand. Second, the species must have thermodynamic data available in either SUPCRTBL or MINES19, which are internally consistent (Johnson et al., 1992; Zimmer et al., 2016; Gysi et al., 2023). The two databases comprise data from largely the same studies, with MINES19 offering additional species not present in SUPCRTBL, as well as updated data for select species. For details on the uncertainties in the thermodynamic data, when reported, the reader is referred to the SUPCRTBL (Johnson et al., 1992; Zimmer et al., 2016) and MINES19 (Gysi et al., 2023) databases and the references therein. Third, only one chloride, fluoride, or hydroxide species, when available, were selected for each metal in order to decrease the complexity of the system. Fourth, analogous chloride, fluoride, or hydroxide species for individual metals were chosen. For example, in the SUPCRTBL database various chloride species are available for La in the form of $LaCl^{+2}$, $LaCl_2^+$, $LaCl_3$ and $LaCl_4^-$, whereas the hydroxide species available is $LaOH^{+2}$. In such cases were both $LaCl^{+2}$ and $LaOH^{+2}$ were chosen as the species present as they are analogous, i.e. similarly charged. Condition four was violated for the specific case of iron because iron is a major element in many systems, and the Fe^{2+} hydroxide and fluoride single cation/anion species available in SUPCRTBL are $FeOH^+$ and FeF^+, whereas the most relevant iron chloride species available is $FeCl_2$ (other choice is $FeCl^+$); see Scholten et al. (2019) and references therein.

The assumption that each metal-anion pair is only present as one species limits the model's accuracy at P-T-X ranges, wherein the speciation changes. However, how large of an effect this has is unknown because information on the speciation of metals, particularly in complex, multi-component fluids, is known only for select metals (Kouzmanov et al., 2012; Pokrovski et al., 2013; Tattitch and Blundy, 2017). It may be argued that if a metal remains predominantly speciated to a single cation the change in the chloride species of that metal will have a

relatively smaller effect than if the speciation of a metal changes from one anion to another, i.e. chloride to fluoride, where that new metal-anion pair has not been considered. The latter effect may be particularly problematic due to the general incompleteness of thermodynamic databases. If thermodynamic data are not available, species cannot be incorporated into the present model and thus changes in speciation from one anion to another may severely limit the accuracy of the model in some circumstances. Thus, the reliance on existing thermodynamic databases combined with the necessity for simplification is a strong limiting factor and care should be taken when interpreting the results this model to ensure the metals of interest are sufficiently constrained. It is also important to note that the choice of species used in this study does not imply the absences of other species, but merely a simplification of a multicomponent fluid.

All speciation calculations were performed in MATLAB. The scripts, as well as a compiled application (known as SoAP: Solutes in Aqueous Phases), used to perform speciation calculations are provided in a public GitLab repository (https://gitlab.com/agion18/SoAP.git). The speciation calculations performed in this work were compared against similar calculations performed in GEMS (Kulik et al., 2013) for a simple Li-Na-K-F-Cl-H-O system with Li:Na:K:F:Cl ratios of 0.5:1:1:0.1:1 at a temperature of 800°C and pressure of 200 MPa to confirm their accuracy. Aqueous species chosen in GEMS were single anion chloride, fluoride, and hydroxide species. The calculated concentrations of each species in the fluid are within ±10 relative% of GEMS, with the exception of H^+, which is 17% different. Further, all calculated Debye-Hükel activity coefficients for all species were with ±1 relative% of GEMS. In the remaining text all mole fractions of species in the fluid are calculated values based on the bulk composition of that fluid, the chosen fluid species, and existing thermodynamic data.

4.2. Apparent Equilibrium Constants

Apparent equilibrium constants describing the exchange of metals between fluids and silicate melts are typically calculated (Holland, 1972) as e.g.

$$\mathrm{K_{K,Na}} = \frac{\mathrm{D_K}}{\mathrm{D_{Na}}} = \frac{C_K^{Fluid} C_{Na}^{Melt}}{C_K^{Melt} C_{Na}^{Fluid}} \quad , \tag{1}$$

Where $\mathrm{K_{K,Na}}$ is the equilibrium constant for the exchange of potassium and sodium, $\mathrm{D_K}$ and $\mathrm{D_{Na}}$ is the fluid/melt partition coefficients for potassium and sodium, respectively and C_i is the concentration of potassium or sodium in the melt or fluid. However, this form does not consider multiple ligands (Cl, F, etc.) or the independent variation of each species in the fluid. Instead of taking this approach, we have utilized the equilibrium concentration of each species, as determined above, to calculate apparent equilibrium constants for the exchange of metals between a fluid and a silicate melt on a species-by-species basis. Such an approach accounts for variations in metal speciation, as well as for changes in fluid and melt composition. For example, the exchange of sodium and potassium between a supercritical fluid or low-salinity vapor and a silicate melt is

$$\mu_{\mathrm{NaCl}}^{\text{Fluid or Vapor}} + \mu_{\mathrm{KO_{0.5}}}^{\text{Melt}} \rightleftharpoons \mu_{\mathrm{KCl}}^{\text{Fluid or Vapor}} + \mu_{\mathrm{NaO_{0.5}}}^{\text{Melt}} \quad , \tag{2}$$

where μ is the chemical potential of the species or oxide in the fluid/vapor or melt. The relationship between the chemical potential of a component in a solution is expressed by $\mu = \mu^0 + \mathrm{RT ln}\, a$, where μ^0 is the standard state chemical potential of the pure component, and a the activity of the component in a solution, R is the gas constant, and T is temperature in Kelvin. The exchange in equation 2 can then be accurately described by the equilibrium constant ($\mathrm{K_{KCl}}$) using the activities of the components, i.e. species in the melt or fluid, by

$$K_{KCl} = \frac{a_{KCl}^{\text{Fluid or Vapor}} \cdot a_{NaO_{0.5}}^{\text{Melt}}}{a_{NaCl}^{\text{Fluid or Vapor}} \cdot a_{KO_{0.5}}^{\text{Melt}}} \quad , \tag{3a}$$

where a is the activity of the aqueous species in the fluid/vapor or oxide in the melt and is manipulated into the apparent equilibrium constant (K'_{KCl})

$$K'_{KCl} = K_{KCl} \frac{\gamma_{NaCl}^{\text{Fluid or Vapor}} \cdot \gamma_{KO_{0.5}}^{\text{Melt}}}{\gamma_{KCl}^{\text{Fluid or Vapor}} \cdot \gamma_{NaO_{0.5}}^{\text{Melt}}} = \frac{X_{KCl}^{\text{Fluid or Vapor}} \cdot X_{NaO_{0.5}}^{\text{Melt}}}{X_{NaCl}^{\text{Fluid or Vapor}} \cdot X_{KO_{0.5}}^{\text{Melt}}} \quad , \tag{3b}$$

where $X^{Fluid\ or\ Vapor}$ is the mole fraction of a given species on a single cation basis in the fluid/vapor calculated as described in section 4.1 and X^{Melt} is the mole fraction of a given oxide in the melt on a single cation and volatile free basis. We use this approach in a generalized way to link the behavior of major and trace elements in multicomponent systems. Apparent equilibrium constants are calculated from the mole fractions and do not require the activities or activity coefficients to be known. The general form of the equilibrium is for a supercritical fluid or low-salinity vapor

$$z\left(\mu_{Na(Cl,F,OH,+)}^{\text{Fluid or Vapor}}\right) + \mu_{MeO_{0.5z}}^{\text{Melt}} \rightleftharpoons \mu_{i\ or\ j}^{\text{Fluid or Vapor}} + z\left(\mu_{NaO_{0.5}}^{\text{Melt}}\right) \tag{4}$$

and the apparent equilibrium constant is

$$K'_{i\ or\ j} = \frac{X_{i\ or\ j}^{\text{Fluid or Vapor}} \cdot \left(X_{NaO_{0.5}}^{\text{Melt}}\right)^{z}}{\left(X_{Na(Cl,F,OH,+)}^{\text{Fluid or Vapor}}\right)^{z} \cdot X_{MeO_{0.5z}}^{\text{Melt}}} \quad , \tag{5}$$

where *i* is the chloride, fluoride, or hydroxide species and *j* is free cation species (e.g. Na^+, K^+, Ca^{2+}) of interest in the supercritical fluid or vapor; $MeO_{0.5z}$ is the appropriate oxide component in the melt; z is the stoichiometric coefficient required to balance the equilibria and is equal to the charge of the cation in species *i* (e.g. for $CaCl_2$, z = 2). Note, that for simplicity, the apparent equilibrium constants that have a non-neutral charge are calculated as, for example,

$$3\mu_{NaCl}^{\text{Fluid or Vapor}} + \mu_{LaO_{1.5}}^{\text{Melt}} = \mu_{LaCl^{+2}}^{\text{Fluid or Vapor}} + 2\mu_{Cl^-}^{\text{Fluid or Vapor}} + 3\mu_{NaO_{0.5}}^{\text{Melt}} , \tag{6a}$$

$$K''_{LaCl^{+2}} = \frac{X_{LaCl^{+2}}^{\text{Fluid or Vapor}} \cdot \left(X_{NaO_{0.5}}^{\text{Melt}}\right)^{3}}{\left(X_{NaCl}^{\text{Fluid or Vapor}}\right)^{3} \cdot X_{LaO_{1.5}}^{\text{Melt}}} \quad , \tag{6b}$$

where

$$K''_{LaCl^{+2}} = \frac{K'_{LaCl^{+2}}}{(X_{Cl^-})^2} \quad . \tag{6c}$$

For convenience and from this point forward, we will use the symbol $\mathbf{K_i'}$ when referring to apparent equilibrium constants where *i* is a metal or hydrogen species in the fluid and each $\mathbf{K_i'}$ refers to the exchange of a metal or hydrogen (see section below) with sodium as either a chloride, fluoride, hydroxide, or free cation species.

4.3. Hydrogen and the Hydrous Melt Component

Where hydrogen is the main cation (HCl, HF, and H_2O), it is necessary to consider the hydrous aluminosilicate component in the melt as previously used by Candela (1990), Williams et al. (1997), and Frank et al. (2003). The hydrous aluminosilicate component of the melt was originally defined by Candela (1990) for peraluminous systems and describes the excess aluminosilicate component charge balanced by hydrogen instead of Na, K, or Ca. This fictive hydrous aluminosilicate component ($\mathrm{H(fasc)^{Melt}}$) is a stoichiometric convenience and does not need to have structural significance and is calculated as

$$\mathrm{H(fasc)^{Melt}} = \mathrm{C_{Al}^{Melt}} - \left(\mathrm{C_{Na}^{Melt}} + \mathrm{C_{K}^{Melt}} + 2\mathrm{C_{Ca}^{Melt}}\right) \quad , \qquad (7)$$

where C is the concentration of aluminum, sodium, potassium, and calcium in moles per kilogram of melt. Utilizing this component, the apparent equilibrium constant for the exchange of hydrogen with sodium can be written as

$$\mu_{\mathrm{NaCl}}^{\text{Fluid or Vapor}} + \mu_{\mathrm{H(fasc)}}^{\mathrm{Melt}} = \mu_{\mathrm{HCl}}^{\text{Fluid or Vapor}} + \mu_{\mathrm{NaAlO_2}}^{\mathrm{Melt}} \quad , \qquad (8a)$$

$$\mathrm{K'_{HCl}} = \frac{\mathrm{X_{HCl}^{Fluid\ or\ Vapor}} \cdot \mathrm{NaAlO_2^{Melt}}}{\mathrm{X_{NaCl}^{Fluid\ or\ Vapor}} \cdot \mathrm{H(fasc)^{Melt}}} \quad , \qquad (8b)$$

where $X_{\mathrm{HCl}}^{\mathrm{Fluid}}$ is the mole fraction of HCl in the supercritical fluid or vapor phase and $\mathrm{NaAlO_2^{Melt}}$ and $\mathrm{H(fasc)^{Melt}}$ are in the same mole-based concentration units. Other expressions may be written to describe the equilibria of HCl with a silicate melt and the reader is referred to the supplementary information for additional information on the choice of equation 8 and the $\mathrm{H(fasc)^{Melt}}$ parameter. Analytically, $\mathrm{NaAlO_2^{Melt}}$ can be expressed as the concentration of sodium in the melt. However, this definition is limited to peraluminous systems, because when $\mathrm{C_{Al}^{Melt}} < \left(\mathrm{C_{Na}^{Melt}} + \mathrm{C_{K}^{Melt}} + 2\mathrm{C_{Ca}^{Melt}}\right)$, $\mathrm{H(fasc)^{Melt}}$ becomes negative. Therefore, we reconsider the definition of $\mathrm{H(fasc)^{Melt}}$. Note that we change from aluminosilicate components to aluminate components is for simplicity and to allow more flexibility in the model of Candela (1990); however, it is assumed the aluminate components are part of the silicate melt structure.

In the original definition of $\mathrm{H(fasc)^{Melt}}$, the hydrogen in the melt either charge balances the aluminum-silicate complexes or is present as H_2O. However, hydrogen may be present as both H_2O and OH groups (Farnan et al., 1987; Zeng et al., 1999, 2000; Xue and Kanzaki, 2007; Le Losq et al., 2015). Considering only major element hydroxide complexes, the hydrogen mass balance is defined as

$$\sum \mathrm{H^{Melt}} = 2\mathrm{H_2O_m^{Melt}} + \mathrm{KOH^{Melt}} + \mathrm{NaOH^{Melt}} + \mathrm{H(fasc)^{Melt}} + \mathrm{SiOH^{Melt}} + 2\mathrm{Ca(OH)_2^{Melt}} \quad , (9)$$

where $\mathrm{H_2O_m^{Melt}}$ is molecular water in the melt. The mass balances for Al, Na, K and Ca, in moles per kilogram of melt, are thus

$$\sum \mathrm{Al}^{\mathrm{Melt}} = \mathrm{NaAlO_2^{Melt}} + \mathrm{KAlO_2^{Melt}} + \mathrm{H(fasc)^{Melt}} + 2\mathrm{CaAl_2O_4^{Melt}} \quad , \quad (10)$$

$$\sum \mathrm{Na}^{\mathrm{Melt}} = \mathrm{NaAlO_2^{Melt}} + \mathrm{NaOH^{Melt}} \quad , \quad (11)$$

$$\sum \mathrm{K}^{\mathrm{Melt}} = \mathrm{KAlO_2^{Melt}} + \mathrm{KOH^{Melt}} \quad , \quad (12)$$

and

$$\sum \mathrm{Ca}^{\mathrm{Melt}} = \mathrm{CaAl_2O_4^{Melt}} + \mathrm{Ca(OH)_2^{Melt}} \quad . \quad (13)$$

Equations (9) and (10) can be re-arranged and added together to yield

$$2\mathrm{H(fasc)^{Melt}} = \sum \mathrm{Al}^{\mathrm{Melt}} - \sum \mathrm{Na}^{\mathrm{Melt}} - \sum \mathrm{K}^{\mathrm{Melt}} - 2\sum \mathrm{Ca}^{\mathrm{Melt}} + \sum \mathrm{H}^{\mathrm{Melt}} - 2\mathrm{H_2O_m^{Melt}} - \mathrm{SiOH^{Melt}} \quad . \quad (14)$$

The total amount of Al, Na, K, and Ca was measured through standard electron microprobe analyses. The amount of molecular water was determined by considering the equilibrium

$$\mathrm{H_2O_m^{Melt}} + \mathrm{O^{Melt}} \rightleftharpoons 2\mathrm{OH^{Melt}} \quad (15)$$

and the equilibrium constant from Stolper (1982) of

$$\mathrm{K_{H_2O}^{Melt}} = \frac{\mathrm{X_{OH}^{Melt}}^2}{\mathrm{X_{H_2O_m}^{Melt}} \cdot \mathrm{X_O^{Melt}}} \quad , \quad (16)$$

where $\mathrm{X_{OH}^{Melt}}$, $\mathrm{X_{H_2O_m}^{Melt}}$, and $\mathrm{X_O^{Melt}}$ are the mole fractions of hydroxyl, molecular water, and anhydrous oxygen and are approximations of their respective activities. The mole fractions were iteratively calculated for by using equation (3) of Zhang and Ni (2010) and by assuming a $\mathrm{K_{H_2O}^{Melt}}$ of 0.553 for a temperature of 800°C as calculated from the best-fit regression of Nowak and Behrens (2001), which has an uncertainty of ±15%.

In regards to $\mathrm{SiOH^{Melt}}$, Zeng et al. (2000) observed multiple AlOH and SiOH groups, as well as Al-OH-Si groups in the melt, and determined that both SiOH/$\sum$ OH and AlOH/$\sum$ OH vary as a function of the Si/Al ratio of the melt in a power law relationship, such that increasing Si/Al increases SiOH/$\sum$ OH and decrease AlOH/$\sum$ OH. By utilizing the model and data of Zeng et al. (2000), and assuming that all Al-OH-Si groups were counted as AlOH groups, their data were refitted to show that SiOH/AlOH also vary as a function of Si/Al in a power law relationship where increasing Si/Al increases SiOH/AlOH such that

$$R_{\frac{SiOH}{AlOH}}^{Melt} = 6.098 \cdot \left(\left(\frac{Si}{Al}\right)^{Melt}\right)^{0.04081} - 5.56 \quad , \quad (17)$$

where $R_{\frac{SiOH}{AlOH}}^{Melt}$ is the ratio of SiOH groups to AlOH groups. Additionally, because all Al-OH-Si are considered AlOH groups the sum of all AlOH groups is equivalent to $H(fasc)^{Melt}$.

Equation (14) was then written as

$$H(fasc)^{Melt} = \frac{\sum Al^{Melt} - \sum Na^{Melt} - \sum K^{Melt} - 2\sum Ca^{Melt} + \sum H^{Melt} - 2H_2O_m^{Melt}}{2 + R_{\frac{SiOH}{AlOH}}^{Melt}} \quad , \quad (18)$$

which allows $H(fasc)^{Melt}$ to be calculated for both hydrous peraluminous and peralkaline granitic systems. There are four limitations of this approach. First, the minimum $H(fasc)^{Melt}$ is 0. Second, the maximum $H(fasc)^{Melt}$ is $\sum Al^{Melt}$. Third, because the present formalism is not able to calculate the amount of individual hydroxide species (NaOH, KOH, or $Ca(OH)_2$) from bulk composition of the melt alone, the use of the concentration of sodium in the melt to approximate $NaAlO_2^{Melt}$ in equation 8 is still required. Fourth, the choice of $K_{H_2O}^{Melt}$ is vitally important. In sufficiently hydrated melts, a $K_{H_2O}^{Melt}$ that is too large may result in $H(fasc)^{Melt} > \sum Al^{Melt}$, because a large $K_{H_2O}^{Melt}$ results in a larger amount of OH groups, such that

$$\sum OH^{Melt} > \left(R_{SiOH/AlOH}^{Melt} + 1\right)\sum Al^{Melt} + \sum Na^{Melt} + \sum K^{Melt} + 2\sum Ca^{Melt} . \quad (19)$$

For example, for the Bishop Tuff with 12 wt.% water a $K_{H_2O}^{Melt}$ of 0.253 results in X_{OH}^{Melt} of 0.15 and $H(fasc)^{Melt} < \sum Al^{Melt}$, whereas a $K_{H_2O}^{Melt}$ of 0.290 results in X_{OH}^{Melt} of 0.175 and $H(fasc)^{Melt} > \sum Al^{Melt}$. In such cases, $K_{H_2O}^{Melt}$ should be re-evaluated and, if reasonable, constrained such that $H(fasc)^{Melt}$ is infinitesimally smaller than $\sum Al^{Melt}$. Further, in sufficiently dry melts (<1 wt.%, but exact threshold is a function of melt composition), a negative $H(fasc)^{Melt}$ can be calculated, which indicates that a hydrous alumina group may not be present.

4.4. Linking Fluid and Melt Thermodynamic Models

We link currently existing models with the theoretical framework presented in this section in order to construct a model for calculating the composition of magmatic fluids in equilibrium with silicate melts. We combine apparent equilibrium constants, excluding those for free cation species, determined in this work with 1.) MELTS (alphaMELTS for MATLAB) (Ghiorso and Sack, 1995; Gualda et al., 2012; Ghiorso and Gualda, 2015; Antoshechkina and Ghiorso, 2018), 2.) crystal-melt partition coefficients 3.) solubilities of halite (Thomas and Wood, 2023) and fluorite (Dolejš and Baker, 2006) and 4.) the behavior of NaCl (Tattitch et al., 2021).

A flow chart and step-by-step processes of the model and calculation procedure is given in Supplementary Fig. S1 and S2 and the MATLAB code is provided at https://gitlab.com/agion18/fluids.git. The available code can be used for modelling magmatic-hydrothermal systems where coexisting phases include a melt, crystals, and a

supercritical fluid or vapor. An additional add-on is included with the source code to calculated the compositions of coexisting vapors and brine based on previously reported vapor-brine partition coefficients and the H_2O-NaCl phase properties of Driesner and Heinrich (2007) and Driesner (2007). However, this portion of the model is not the focus of the current study and has not been refined using new experimental data and thus is described elsewhere in the supplementary information. All calculations are limited to CO_2 and sulfur-free systems. The model inputs (P-T-X) and calculation options (equilibrium crystallization, fractionation crystallization, etc.) are the same as those required for alphaMELTS, with the addition of crystal-melt partition coefficients. All calculations are iterative and alternate between FLUIDS (i.e. fluid-melt equilibrium code) and MELTS calculations. Crystal-melt trace element partitioning is calculated as a batch process, where all required parameters are updated at each P-T step, and partition coefficients are supplied by the user.

Fluid-melt equilibrium is an optimization problem that is solved with the *fmincon* MATLAB function. The *fmincon* function is built-in MATLAB minimization function that can be used to find the minimum of constrained nonlinear multivariable problems. The FLUIDS calculation searches for the optimal $X_{\mathrm{HCl}}^{\text{Fluid or Vapor}}$ and $X_{\mathrm{HF}}^{\text{Fluid or Vapor}}$ (see results and discussion section for the variation of apparent equilibrium constants with HCl and HF), as well as $X_{\mathrm{H_2O}}^{\text{Fluid or Vapor}}$ and the moles of fluid/vapor, that minimize the difference between the calculated and ideal values of four parameters and considering nonlinear constraints. The ideal parameters are those required to close mass balance and constrain behavior of chlorine and fluorine in melt-vapor (±brine; see supplementary information). These parameters are: 1) Total moles in the system, 2) Moles of hydrogen in the fluid, 3) Chlorine concentration in the melt, and 4) Fluorine concentration in the melt. The differences between the modelled and ideal parameters are aggregated into a scalar by taking the square root of the sum of the squares, which is the value minimized by the *fmincon* solver.

Parameter one is defined by a mass balance equation for the total number of moles in the system. Parameter two is defined by the solubility of water in the melt as calculated by MELTS where any hydrogen in the system not in the melt is present in the fluid. Parameter three is defined by the ideal concentration of chlorine in the melt calculated from the equation of Thomas and Wood (2023):

$$\log_{10} Cl^{-} = \log_{10} a_{NaCl}^{Melt} + 0.06 - \frac{2431X_{Ca}^{Melt}+3430X_{Si}^{Melt}-2592X_{Fe}^{Melt}+3484X_{Na}^{Melt}+4092X_{K}^{Melt}-2417}{T} \quad , \quad (20)$$

where Cl^- is the chlorine concentration in the melt in wt.%, $a_{\mathrm{NaCl}}^{\mathrm{Melt}}$ is the activity of NaCl in the melt, X_h^{Melt} is the mole fraction of element h in the melt on a single-cation and anhydrous basis, and T is temperature in Kelvin. The activity of NaCl in the melt is calculated from the equilibrium

$$\mu_{\mathrm{NaCl}}^{\mathrm{Melt}} = \mu_{\mathrm{NaCl}}^{\text{Fluid or Vapor}} \quad (21)$$

and the resulting equilibrium constant

$$\mathrm{K'_{NaCl}} = \frac{\mathrm{x}_{\text{NaCl equiv.}}^{\text{Fluid or Vapor}}}{\mathrm{a}_{\mathrm{NaCl}}^{\mathrm{Melt}}} \quad , \quad (22)$$

where $X_{\text{NaCl equiv.}}^{\text{Fluid or Vapor}}$ is the mole fraction of NaCl equivalent in the supercritical fluid or vapor. The NaCl equiv. is calculated from all non-water solvent species where $MeCl_z = \frac{1+z}{2}\text{NaCl equiv.}$, e.g. 1 mole $FeCl_2$ equals 1.5 moles NaCl equiv. as recommended by Tattitch and Blundy (2017). This is done to calculate the effective salinity, which is a colligative property, of fluids which may have significant salts that contain cations with >1+ charges. K'_{NaCl} was calculated from the experiments performed in this work and the calibration dataset of Tattitch et al. (2021), where $X_{\text{NaCl equiv.}}^{\text{Fluid or Vapor}}$ is known and $a_{\text{NaCl}}^{\text{Melt}}$ is calculated from the measured chlorine concentration in the melt (equation (20)). K'_{NaCl} with varies the density of fluid phase (Fig. 1) and is described by

$$\log_{10} K'_{\text{NaCl}} = -2.47(\pm 0.23) \cdot 10^{\left(\rho \cdot \frac{-5.9(\pm 0.1)}{10000}\right)} , \quad (23)$$

where ρ is the density of the fluid in kg/m^3 as calculated from the equations of Driesner (2007). In FLUIDS $a_{\text{NaCl}}^{\text{Melt}}$ is calculated from $X_{\text{NaCl equiv.}}^{\text{Fluid or Vapor}}$ and K'_{NaCl} is known at a given P-T condition. The relationship between the K'_{NaCl} and ρ is consistent with previous observations on the relationship between fluid density and thermodynamic properties, as well as ionization constants of solutes such as NaCl, see for example Mesmer et al. (1988), Anderson et al. (1991), and related studies. In cases where $a_{\text{NaCl}}^{\text{Melt}} = 1$ and there is chlorine that can neither be accommodated in the melt or in the fluid phase as defined by equation 22 and excess chlorine phase is defined. This excess chlorine phase may be interpreted as either: 1) a misfit in equation 23; 2) deviation from the relationship of $a_{\text{NaCl}}^{\text{Melt}}$ and Cl in the melt defined in equation 20; or 3) presence of a chlorine-bearing mineral, which are not considered by MELTS, or halite saturation if the fluid phases sufficiently saline, see Driesner and Heinrich (2007).

Parameter four is defined by the ideal concentration of fluorine in melt calculated from the equations of Dolejš and Baker (2006), reproduced here as equation 24a-d:

$$K'_{\text{Fluorite}} = \frac{a_{CaF_2}^{\text{Melt}}}{X_{(CaO)}^{\text{Melt}} \cdot \left(X_{(F_2O_{-1})}^{\text{Melt}}\right)^c} , \quad (24a)$$

where $a_{\text{Fluorite}}^{\text{Melt}}$ is the activity of fluorite in the melt and $X_{(CaO)}^{\text{Melt}}$ and $X_{(F_2O_{-1})}^{\text{Melt}}$ are anion fractions on an anhydrous basis and

$$\log_{10} K'_{\text{Fluorite}} = -2.449 Al_2O_3^{\text{exc}} + 4.902 , \quad (24b)$$

$$c = -0.92 Al_2O_3^{\text{exc}} + 4.902 , \text{ and} \quad (24c)$$

$$Al_2O_3^{\text{exc}} = Al_2O_3 - Na_2O - K_2O . \quad (24d)$$

Where $Al_2O_3^{exc}$, and Al_2O_3, Na_2O, and K_2O are in number of moles per hundred anions on an anhydrous basis. The $a_{CaF_2}^{Melt}$ can also be calculated from the equilibrium

$$K'_{(2)\ \text{Fluorite}} = \frac{X_{CaCl_2}^{\text{Fluid or Vapor}} \cdot \left(X_{HF}^{\text{Fluid or Vapor}}\right)^2}{a_{CaF_2}^{Melt} \cdot \left(X_{HCl}^{\text{Fluid or Vapor}}\right)^2} \quad , \tag{25}$$

where $K'_{(2)\ \text{Fluorite}}$ is approximately 10^4 and calculated from fluorite saturated Bishop Tuff experiments from this work (BT-3-5, BT-4-2, and BT-4-5) where $a_{CaF_2}^{Melt}$ = 1 and the fluid composition in known.

In order to solve the system of equations described above an initial guess of HCl and HF mole fractions is required. The initial guess for the *fmincon* solver is chosen by evaluating a grid of $X_{HCl}^{\text{Fluid or Vapor}}$ and $X_{HF}^{\text{Fluid or Vapor}}$ values ranging from 10^{-10} to 10^{-2} and from 10^{-8} to 10^{-2}, respectively and finding the minimum. The reader is referred the "Results and Discussion" section for the variation of K'_i with $X_{HCl}^{\text{Fluid or Vapor}}$ and $X_{HF}^{\text{Fluid or Vapor}}$. The starting value for $X_{H_2O}^{\text{Fluid or Vapor}}$ is 0.9. The starting point for the moles of fluid/vapor is the number of moles of water in the system that are not dissolved in the melt. Once the starting point is selected the calculation proceed as shown in Supplementary Fig. S1.

The mole fraction of all melt components, except for sodium, wherein the output of MELTS is used, is calculated by FLUIDS by:

$$n_l^{Total} = n_l^{Melt} + n_l^{\text{Fluid or Vapor}} \quad , \tag{26a}$$

which is equivalent to

$$n_l^{Total} = X_{MeO_{0.5z}}^{Melt} \sum n^{Melt} + X_i^{\text{Fluid or Vapor}} \sum n^{\text{Fluid or Vapor}} \, . \tag{26b}$$

The mole fraction of each metal can then be solved for as shown in equation 27.

$$X_{MeO_{0.5z}}^{Melt} = \frac{n_l^{Total}}{\sum n^{Melt} + \frac{X_i^{\text{Fluid or Vapor}}}{X_{MeO_{0.5z}}^{Melt}} \sum n^{\text{Fluid or Vapor}}} \quad , \tag{27}$$

where ratios of all species-melt oxide pairs are calculated from their respective apparent equilibrium constants.

5. Results and Discussions

5.1. General Experimental Observations

Experimental run products are primarily crystal-free glasses and a fluid. In some fluorine-bearing Bishop Tuff experiments there is minor quartz with clusters of biotite and fluorite ± alkali feldspars all with sizes of <~10 microns (Fig. S3). The glasses are hydrated equivalents (Supplementary Tables S1-S3) of the starting materials with modified sodium, potassium, chlorine, and fluorine concentrations due to equilibration with the chloride solutions (Fig. 2 and Supplementary Table S3). The Na/K ratio of the run product melts progressively decreases and the

chlorine concentration in the melt increases as the fluids become more NaCl- and KCl-rich (Fig. 2A). The trace elements concentrations in the melt slightly decrease, e.g. Li and Rb, with increasing salinity of the fluid (Fig. 3) but are generally constant. This decrease is the result of both 1) the dilution of the trace elements due to dissolution of water in the melt and 2) mass transfer of metals from the melt into the fluid. The mass transfer of metals from melt to fluid is relatively minor and is supported by the observation that the starting fluid phase and supercritical phase at pressure and temperature have roughly constant masses even in experiments with >1 *m*Cl (Table 1). All fluids are representative of low-salinity (<11 wt.% NaCl equiv, i.e. <3 molal NaCl equiv.; Fig. 4), supercritical phases (Driesner and Heinrich, 2007). Fluids are predominantly sodium- and potassium-rich (Supplementary Table S3) and contain significant (thousands of ppm) Mg, Al, Si, Ca, and Fe (Fig. 5). The fluids also contain trace metals ranging from tens to several hundreds of ppm of Li, B, F, Cr, Mn, Co, Ni, Cu, Zn, Ga, Rb, La, Ba, and Pb; less than 1 ppm of Be, Sc, Sr, Y, REEs, Zr, Nb, Mo, Cd, Sb, and Hf; or are below detection in the case of Ge, Th, and U (Fig. 5). Fluids in Macusani-bearing experiments can also contain up to thousands of ppm Li, B, and F. The variation in run product fluid chemistry, is primarily a function of the fluid salinity and, generally, the concentration of the trace elements in the fluid increases within increasing salinity (Fig 5). Note, data from several of the experiments (BT-1-S4, BT-1-S5, BT-2-S4, BT-12-S5, BT-4-2-S4, and BT-7-S4) discussed in Gion et al. (2022) have been incorporated in this study and thus those data are included herein and in the supplementary files for completeness.

In order to remain consistent with the literature we report partition coefficients for all metals of interest (Fig. 6, Supplementary Fig. S4, and Supplementary Table S4). However, if we compare, for example $D_{Li}^{Fluid/Melt}$, from this work and previous studies (Webster et al., 1989; Bos, 1990; Iveson et al., 2019) (Fig. 7), we find that the relationship of $D_{Li}^{Fluid/Melt}$ to m_{Cl}^{Fluid} varies from study-to-study, such that a given $D_{Li}^{Fluid/Melt}$ does not correspond to a specific salinity (Fig. 7). The discrepancy between studies can be explained by a simple thought experiment wherein a melt has 1 mol/kg of sodium, 0.1 mol/kg lithium, and assume $D_{Li}^{Fluid/Melt} = 1 m_{Cl}^{Fluid}$. For a fluid with 1 *m*Cl, there is then 0.1 *m*LiCl in the fluid and the remaining chlorine is present as 0.9 *m*NaCl. If 0.5 *m*CuCl is added to the fluid, and assuming it stays in the fluid phase, the chlorine content of that fluid is now 1.5 *m*Cl (0.1 *m*LiCl + 0.9 *m*NaCl + 0.5 *m*CuCl). In this scenario lithium cannot increase in the fluid because no chlorine is available to balance it and the initial relationship of $D_{Li}^{Fluid/Melt} = 1 m_{Cl}^{Fluid}$ is no longer valid. Instead $D_{Li}^{Fluid/Melt} = 0.66\, m_{Cl}^{Fluid}$ demonstrating that chloride-dependent partition coefficients are not generally applicable because Li and Cl are not independently variable components. Therefore, the choice for $D_{Li}^{Fluid/Melt}$ can be made somewhat arbitrarily and a more thermodynamically rigorous approach is needed.

5.2. Approach to Equilibrium

Equilibrium between the fluid and silicate melt was evaluated by considering the homogeneity of the melt. The major and trace element composition of the melt typically varies by <10 relative percent (Supplementary Table 1). Additionally, the homogeneity of the melt from rim-to-core can be qualitatively evaluated by performing semi-quantitative energy dispersive spectroscopy (EDS) line scans (two per glass) for select glasses by using a ZEISS Merlin Compact SEM (Fig. S5). A subset of these lines scans (BT-2-S5, BT-2-S4, and BT-7) were previously discussed in Gion et al. (2022) and those results are expanded upon here.

The Si/Na and Na/K can be used to evaluate if the melt reached equilibrium with the fluid phase during the experiment and if the composition of the glass and fluid were modified during quench. Generally, in rhyolitic melts silicon is one of the slowest diffusing elements and sodium and potassium are one of the fastest diffusing elements (Zhang et al., 2010). In these experiments, there is significant exchange of the alkalis with the fluid (Fig. 2A) and some exchange of silicon, although silicon in the fluid was not explicitly measured. Therefore, if diffusive equilibration was not reached, the Si/Na ratio of the glass should show a systematic change from rim-to-core because the rate at which they diffuse is significantly different. However, there is no systematic variation in Si/Na ratios from rim-to-core and changes in the Si/Na show no variation. Additionally, the change in the silicon concentration from rim-to-core is <5 relative percent with only a few experiments (Mac-5-S4 and Mac-8) exhibiting an increase in silicon at the rim. Thus, there is weak evidence for disequilibrium and thus we concluded that the fluid and melt have reached equilibrium by diffusion (Fig. S5). Furthermore, the glass frequently contained vesicles and thus the length scale of diffusion may not be the length of the entire glass chip (mm scale) but may be on the

order of the tens to hundreds of microns as the melt locally equilibrates with the fluid. We have previously shown that in these experiments the Na/K ratio is constant in Bishop Tuff experiments and that there is no evidence for ion-exchange during both slow and rapid quench (Gion et al., 2022), as previously reported by Shinohara et al. (1989). We find similar results for the Macusani experiments performed herein and conclude that there is little to no modification of the fluid and/or glass composition during slow or rapid quench.

Equilibrium can also be evaluated by examining the variation of the partition coefficients with time. Partition coefficients for selected elements from fluorine-free Bishop Tuff experiments where solution S4 (Tables 2 and 3) was used are plotted as a function of run time in Fig. 8A and Macusani experiments in Fig. 8B. These experiments were selected because solution S4 was used in the majority of experiments and therefore the bulk salinity of these runs was constant, thus removing the effect of salinity on partition coefficients. Partition coefficients tend to be more variable at shorter run times. We also observe a slight increase in the partition coefficient for Cu for Bishop Tuff experiments with time; however, there is no significant variation in partition coefficients after ~5 days for Li, Na, K, Cl, Zn, Fe, Mn, Nd, and Cu in Macusani experiments with time, consistent with an approach toward equilibrium.

In addition to equilibration of the fluid with the melt, it is also necessary to examine equilibration of the melt/fluid with the gold capsule to determine if the system is truly closed or if there is migration of metals into or out of the capsule walls. Mass balance calculations were performed as described in Gion et al. (2022) wherein the composition of the fluid phase was calculated from the composition and measured masses of the starting materials and the run product glasses and fluids. A comparison of measured and calculated fluid compositions for select elements is provided in Fig. 9. Fig. 9 clearly indicates that for most elements mass balances are inaccurate for determining the compositions of experimental fluids, particularly for metals that occur at concentrations of <1000 ppm. This observation is consistent with the studies of Iveson et al. (2019) and Gion et al. (2022), who observed that uncertainties in mass balance calculations may arise from a variety of sources including poor estimations of the mass fractions of crystalline phases that may sequester metals, contamination during capsule preparation, and the trace element contents of noble metal capsules. Additionally, there is a significant influx of elements like nickel, chromium, and vanadium into the system, which translates into high concentrations in the run product fluids, despite the dearth of these element in the starting materials. Such elements are highly abundant in metal alloys that are frequently found in experimental laboratories in the form of tools and equipment, including the superalloys used for the construction of pressure vessels; thus, contamination is unsurprising. The discrepancy between measured and calculated fluid composition is less apparent for alkali metals, although mass balance calculations tend to overestimate sodium and potassium, likely due to the crystallization of minor phases (feldspars) that are unaccounted for due to their small crystal size and unknown proportions. There is strong agreement between measured and calculated measured chlorine contents of the fluid, which is consistent with a complete recovery of the fluid phase and its solute load because chlorine is strongly compatible in the fluid relative to all other phases. Thus, measured compositions of the fluids provide are a more robust and reliable than mass balance calculations.

5.3. Variation of Apparent Equilibrium Constants

We calculated K_i''s from the equilibrium concentration of 129 aqueous species present in the fluid (Supplementary Tables S5-S7), which are summarized in Fig. 6, as well as Supplementary Fig. S4, and are provided in Supplementary Tables S8-S12. If K_i' is less than one, the reactants (metal oxides in the melt, e.g. $KO_{0.5}$ and a sodium-species in the fluid, e.g. NaCl) are favored over the products (metal species in the fluid, e.g. KCl and sodium oxide in the melt, e.g. $NaO_{0.5}$), whereas if K_i' is greater than one the products are favored. Apparent equilibrium constants vary depending on the metal-ligand pair. In general, monovalent and trivalent chlorides and most free cations have K_i' of less than one (Fig. 6), whereas divalent chlorides and most fluorides and hydroxides have K_i' values of equal to or greater than one (Fig. 6).

We find that K_i' is a function of the HCl and HF content of the fluid (Fig. 10), such that K_i' can either increase or decrease with increasing HCl and increases with increasing HF. The change of K_i' with HCl was interpreted by Frank et al. (2003) to be the result of HCl neutralization by NaOH groups in the melt, which we have expanded to include any metal hydroxide group present in the melt

586 $$\mathrm{z(HCl^{Fluid\ or\ Vapor}) + Me(OH)_z^{Melt} \rightleftharpoons MeCl_z^{Fluid\ or\ Vapor} + zH_2O} \quad , \quad (28)$$

587

588 where $\mathrm{Me(OH)_z^{Melt}}$ is a metal hydroxide complex in the melt and $\mathrm{MeCl_z^{Fluid\ or\ Vapor}}$ is the corresponding metal
589 chloride in the fluid/vapor phase. The equilibrium constant is then

590

591 $$\mathrm{K_{HCl,Me(OH)_z}} = \frac{X_{\mathrm{MeCl_z}}^{\mathrm{Fluid\ or\ Vapor}} \cdot \left(f_{\mathrm{H_2O}}\right)^z}{\left(X_{\mathrm{HCl}}^{\mathrm{Fluid\ or\ Vapor}}\right)^z \cdot X_{\mathrm{Me(OH)_z}}^{\mathrm{Melt}}} \quad , \quad (29)$$

592

593 where $f_{\mathrm{H_2O}}$ is the fugacity of water. In addition to this we consider the substitution of fluorine into an albitic melt
594 (Dingwell and Mysen, 1985),

595

596 $$\mathrm{bF_2O_{-1}^{Melt} + NaAlSi_3O_8^{Melt} \rightleftharpoons NaAlSi_3O_{8-b}F_{2b}^{Melt}} \quad , \quad (30a)$$

597

598 which can be modified to describe the incomplete substitution of fluorine into the sodium aluminate component of
599 the melt by

600

601 $$b\mathrm{HF^{Fluid\ or\ Vapor}} + \mathrm{NaAlO_2^{Melt} \rightleftharpoons NaAlO_{2-\frac{b}{2}}F_b^{Melt}} + \frac{b}{2}\mathrm{H_2O} \quad , \quad (30b)$$

602

603 where *b* is a stochiometric constant and the equilibrium constant is

604

605 $$\mathrm{K_{NaAlF}} = \frac{X_{\mathrm{NaAlO_{2-\frac{b}{2}}F_b}}^{\mathrm{Melt}} \cdot \left(f_{\mathrm{H_2O}}\right)^{\frac{b}{2}}}{\left(X_{\mathrm{HF}}^{\mathrm{Fluid\ or\ Vapor}}\right)^b \cdot X_{\mathrm{NaAlO_2}}^{\mathrm{Melt}}} \quad . \quad (31)$$

606

607 Considering the general form of the apparent equilibrium constant defined in equation 5, the melt components can
608 be re-defined as

609

610 $$X_{\mathrm{NaO_{0.5}}}^{\mathrm{Melt}} = X_{\mathrm{NaAlO_2}}^{\mathrm{Melt}} + X_{\mathrm{NaOH}}^{\mathrm{Melt}} + X_{\mathrm{NaAlO_{2-\frac{b}{2}}F_b}}^{\mathrm{Melt}} \quad (32a)$$

611 and

$$X^{\mathrm{Melt}}_{\mathrm{MeO_{0.5z}}} = X^{\mathrm{Melt}}_{\mathrm{MeAl_zO_{2z}}} + X^{\mathrm{Melt}}_{\mathrm{Me(OH)_z}} \quad , \tag{32b}$$

where $X^{\mathrm{Melt}}_{\mathrm{MeAl_zO_{2z}}}$ is the corresponding aluminate component in the melt for a metal. Substituting equations (32a) and (32b) into equation (5) and applying binomial theorem then re-arranging yields

$$\mathrm{K}'_i = \frac{\left(1+ \frac{c_1}{x^{\text{Fluid or Vapor}}_{\mathrm{HCl}}} + \mathrm{c}_3\left(X^{\text{Fluid or Vapor}}_{\mathrm{HF}}\right)^b\right)^z}{1+\frac{c_2}{\left(x^{\text{Fluid or Vapor}}_{\mathrm{HCl}}\right)^z.}} \cdot \mathrm{K}'_{0,i} \quad , \tag{33a}$$

where

$$\mathrm{K}'_{0,i} = \frac{X_i^{\text{Fluid or Vapor}} \cdot \left(X^{\mathrm{Melt}}_{\mathrm{NaAlO_2}}\right)^z}{\left(X^{\text{Fluid or Vapor}}_{\mathrm{NaCl}}\right)^z \cdot X^{\mathrm{Melt}}_{\mathrm{MeAl_zO_{2z}}}} \tag{33b}$$

and is the exchange of species *i* between the fluid and the respective aluminate components in the melt (Frank et al., 2003) at infinite dilution of HCl and HF and c_1 , c_2 , c_3, and b are fitted parameters

$$c_1 = \frac{X^{\text{Fluid or Vapor}}_{\mathrm{NaCl}} \cdot f_{\mathrm{H_2O}}}{\mathrm{K}_{\mathrm{HCl,NaOH}} X^{\mathrm{Melt}}_{\mathrm{NaAlO_2}}} \quad , \tag{33c}$$

$$c_2 = \frac{X_i^{\text{Fluid or Vapor}} \cdot \left(f_{\mathrm{H_2O}}\right)^z}{\mathrm{K}_{\mathrm{HCl,Me(OH)_z}} X^{\mathrm{Melt}}_{\mathrm{MeAl_zO_{2z}}}} \quad , \tag{33d}$$

and

$$c_3 = \frac{\mathrm{K}'_{\mathrm{NaAlF}}}{\left(f_{\mathrm{H_2O}}\right)^{\frac{b}{2}}} \quad . \tag{33e}$$

Depending on the values of c_1 and c_2 the apparent equilibrium constants may either decrease or increase with increasing $X_{\mathrm{HCl}}^{\text{Fluid or Vapor}}$. Consider a fluorine-free system $\left(X_{\mathrm{HF}}^{\text{Fluid or Vapor}} = 0\right)$ and a species where z =1. In such systems, as $X_{\mathrm{HCl}}^{\text{Fluid or Vapor}}$ approaches zero, the limit of equation (33a) is

$$\mathrm{K}_{\mathrm{i}}' = \frac{c_1}{c_2} \cdot \mathrm{K}_{0,\mathrm{i}}' \quad . \tag{34}$$

Because c_1 and c_2 are inversely related to the neutralization of HCl by NaOH and other metal hydroxides, if $\mathrm{K}_{\mathrm{HCl,NaOH}} < \left(\mathrm{K}_{\mathrm{HCl,Me(OH)_z}}\right)^{z^{-1}}$, as $X_{\mathrm{HCl}}^{\text{Fluid or Vapor}}$ decreases K_{i}' will increase. Therefore, if c_1 is greater than c_2 as $X_{\mathrm{HCl}}^{\text{Fluid or Vapor}}$ decreases K_{i}' will increase and if c_1 is less than c_2 as $X_{\mathrm{HCl}}^{\text{Fluid or Vapor}}$ decreases K_{i}' will decrease.

We fit our experimental derived data to equation (33a) for all species and generate predictive models for K_{i}' as a function of HCl and HF. The five best fit parameters ($\mathrm{K}_{0,\mathrm{i}}'$, c_1, c_2, c_3, and b) for each species were determined by minimizing the standard error of the regression (SE) with the *ga* function in MATLAB. The SE was calculated as

$$\frac{\sqrt{\sum \left(\log_{10}(K_{fit}) - \log_{10}(K_{exp})\right)^2}}{N-2} \quad , \tag{35}$$

where K_{fit} is the calculated apparent equilibrium constant from equation (33a), K_{exp} is the apparent equilibrium constant calculated from the experimental data (Supplementary Tables S8-S12), and N is the number of experimental observations. The minimization was constrained to reduce the range of c_1, c_3, and b values calculated. This assumption is made because the c_1 and c_3 terms are the same regardless of the species of interest being, i.e. c_1 and c_3 only concern $\mathrm{K}_{\mathrm{HCl,NaOH}}$, $\mathrm{K}_{\mathrm{NaAlF}}'$, $f_{\mathrm{H_2O}}$, and sodium species in the melt and fluid (equation 33c and 33e), but do not concern other metal species. Therefore, for a given set of experiments all of the variables that constitute c_1 and c_3 are the same for all K_{i}'s, whereas in c_2 the melt and fluid species are different for each K_{i}'. The b parameter is a stoichiometric coefficient that, in a given system, should also be constant. This assumption resulted in a bimodal distribution of c_1, c_3, and b, which is likely due to a misfit in other best fit parameters. All fitting parameters including the SE and R^2 values are provided in Supplementary Table S13. Additionally, 3D surface plots of the fits, with experimental observations, are provided as MATLAB figures at https://gitlab.com/agion18/fluids.git.

Calculated apparent equilibrium constants for HCl (Fig. 6; Supplementary Table S12) were supplemented by with the work of Simon et al. (2004) and Williams et al. (1997) (Supplementary Table S14) and increase with decreasing pressure and increase with increasing fluid/(fluid + melt), see Fig. 11. The $\mathrm{K}_{\mathrm{HCl}}'$ can be fit to the equation

$$\log_{10}(\mathrm{K}_{\mathrm{HCl}}') = -5.93(\pm 1.25) + 10^{\mathrm{P}\cdot -0.004(\pm 0.002) + \frac{\text{Fluid or Vapor}}{(\text{Fluid or vapor}) + \text{Melt}} * 1.79(\pm 0.26)} \quad , \tag{36}$$

where P is pressure in MPa and $\frac{\text{Fluid or Vapor}}{\text{(Fluid or vapor) + Melt}}$ is the mass fraction of fluid in the fluid + melt portion of the system. The correlation of $\log_{10}(K'_{HCl,NaCl})$ with pressure is consistent with previous observations (Shinohara and Fujimoto, 1994; Williams et al., 1997; Shinohara, 2009); and is not a function of the quench rate (Shinohara et al., 1989; Gion et al., 2022), see above discussion on equilibrium; or the vapor/(vapor + brine) (Williams et al., 1997) ratio because all experiments were performed in the one-phase field. The variation of K'_{HCl} with fluid/(fluid + melt) is may be an artifact of the experimental design of this and previous studies, which often used high fluid fractions (e.g. >50 wt.%). Such large fluid/(fluid + melt) may affect the K'_{HCl} in one of two ways. First, high fluid/(fluid + melt) values may result in a significant portion of the melt dissolving into the fluid and the production of more HCl, and thus a higher $X_{HCl}^{\text{Fluid or Vapor}}$ relative to $H(fasc)^{Melt}$ as compared to experiments with low fluid/(fluid + melt). Second, it has been observed that HCl does not become a primary species in the fluid phase until the melt reaches the solubility limit of chlorine and there is significant chlorine, such that the amount of chlorine exceeds that of the cations it can speciates with in the fluid (Webster and Holloway, 1988). Thus, in experiments with large fluid/(fluid + melt), wherein that fluid has wt% levels of chlorine it is likely that the melt approaches the solubility limit of chlorine and HCl become a more prominent species. In the context of the experiments performed here, the solubility limit of the Bishop Tuff and the Macusani Rhyolite are ~0.3-0.4 wt% and ~0.4 to 0.6 wt% Cl, respectively (Thomas and Wood, 2023) at the present conditions. The run product glasses have chlorine concentrations far below these values and have ratios of measured/maximum concentrations of chlorine of <0.5 (mean of 0.2). However, the studies of Williams et al. (1997) and Simon et al. (2004) utilize larger fluid/(fluid + melt) and have ratios of measured/maximum concentrations of chlorine of 0.2-1 (mean of 0.6). Further, in the present study the H/(Na+K) ratio is low in the high salinity experiments (solution S4 and S5) such that there is little excess chlorine to form HCl. Conversely, Williams et al. (1997) and Simon et al. (2004) us $HCl/\sum Cl$ from 0.03 to 0.3 in their high salinity experiments, which is 2-3 orders of magnitude greater than solutions S4 and S5. In regards to our low-salinity experiments with solutions S1-S3, the fluid/(fluid + melt) is low enough such that there is a sufficient amount of alkalis in the melt that can be leached and form NaCl or KCl species as opposed to HCl. Thus, inclusion of the fluid/(fluid + melt) term is necessary to compare experiments conducted at different fluid fractions and to account for the either the effect of melt dissolution into the fluid or reaching the solubility limit of chlorine. However, in natural systems the fluid/(fluid + melt) is likely to be <0.5, for example at complete degassing a melt with an initial water content of 15 wt.% will have a maximum fluid/(fluid + melt) of ~0.15. At these low fluid/(fluid + melt) values K'_{HCl} will only vary as a function of pressure and the fluid/(fluid + melt) term has minimal effect. Additionally, $\log_{10}(K'_{HF})$ and $\log_{10}(K'_{H_2O})$ calculated from our experimental results and can be described by a linear relationship ($R^2 = 1$ for both fits) with $\log_{10}(K'_{HCl})$.

$$\log_{10}(K'_{HF}) = \log_{10}(K'_{HCl}) + 3.93 \quad (37)$$

$$\log_{10}(K'_{H_2O}) = \log_{10}(K'_{HCl}) + 9.23 \quad (38)$$

Analytical uncertainties, and assuming negligible uncertainty in the thermodynamic data, translate to a maximum ~20 relative percent for all apparent equilibrium constants.

5.4. Consistency with the Literature

The results of our experiments are broadly consistent with previous studies when compared on the basis of partition coefficients (Holland, 1972; Flynn and Burnham, 1978a; Candela and Holland, 1984; Manning and Henderson, 1984; Urabe, 1987; London et al., 1988; Webster et al., 1989; Bos, 1990; Webster, 1990; Keppler and Wyllie, 1991; Webster, 1992b; Williams et al., 1997; Chevychelov and Chevychelova, 1998; Bai and Koster van Groos, 1999; Schaefer et al., 1999; Reed et al., 2000; Simon et al., 2006; Zajacz et al., 2008; Borchert et al., 2009; Borchert et al., 2010a; Borchert et al., 2010b; Borisova et al., 2012; Zajacz et al., 2012; Pokrovski et al., 2013; Tang

and Zhang, 2015; Tattitch et al., 2015; Tattitch and Blundy, 2017; Iveson et al., 2019; Tattitch et al., 2021) (Fig. 6, Fig S4, and Supplementary Tables 4 and 8-11). The reader is referred to Gion et al. (2022) for a direct comparison of select partition coefficients from several experiments used here. We will restrict this discussion to the comparison of previously determined apparent equilibrium constants. There is, at present, a dearth of studies reporting K'_i for individual species and therefore the K'_i presented in this study are unique among experimental results. Numerous studies have reported ratios of partition coefficients relative to sodium, i.e. equation (1); however, because there is a of lack information of the individual ligands these may be considered "bulk" apparent equilibrium constants. We can then compare K'_i from the current study with previously reported "bulk" apparent equilibrium constants for species that are dominantly chlorides.

The most commonly reported apparent equilibrium constants (eq. 1) are for potassium. Reported bulk apparent equilibrium constants range from 0.45 to 0.75 (Gammon et al., 1969; Holland, 1972; Shinohara et al., 1989; Williams et al., 1997; Schaefer et al., 1999; Student and Bodnar, 1999; Frank et al., 2003; Zajacz et al., 2008), which is consistent with the present study. However, the relationship between K'_{KCl} and X_{HCl}^{Fluid} for low-salinity supercritical fluids that we observe (Fig. 10A) is the opposite trend of that observed by Frank et al. (2003) (Fig. 5 of their study) for high-salinity brines. These differing trends are consistent with $K'_{HCl,NaOH} > K'_{HCl,KOH}$ in vapor-dominated systems and $K'_{HCl,NaOH} < K'_{HCl,KOH}$ in brine-dominated systems, i.e. equation (34). Therefore, when HCl is present in a vapor phase it is a more efficiently neutralized by NaOH in the melt and preferentially produces NaCl, whereas when HCl present in brines it is more efficiently neutralized by KOH in the melt and preferentially produces KCl. This is consistent with the observations of Sublett et al. (2018) who reported that sodium has a slight preference for a low-salinity vapor phase whereas potassium has a slight preference for the high-salinity brine phase. Zajacz et al. (2012) also examined the exchange of potassium between vapor and an andesitic melt and observed an average apparent equilibrium constant of 1.23. Zajacz et al. (2012) noted that in their system there was no correlation with the HCl content of the fluid and that the apparent equilibrium constant was greater than in felsic systems. In regard to the lack of correlation with HCl, we suggest that the HCl content of the fluid was too large to capture this effect. Zajacz et al. (2012) reported $m\mathrm{HCl} > 2 \cdot 10^{-4}$, whereas in our study we observe the effect of HCl at $X_{HCl}^{Fluid} \cong 10^{-6} \cong m\mathrm{HCl}$ and values significantly higher than this will produce an equilibrium constant defined by $K'_{ex,(KCl)}$ (equation (33b)). The effect of temperature may also play a role because experiments in many felsic system are performed at <900°C, whereas the experiments of Zajacz et al. (2012) were performed at 1000°C. Further, the variation of activity coefficients in the melt components with P-T-X parameters is unknown, which may result in variable apparent equilibrium constants.

Apparent equilibrium constants, as ratios of partition coefficients, have also been reported for Li, Be, Rb, Sr, Fe, Cu, Ca, Mg, Mn, Zn, U, Th and REEs in supercritical or vapor phases. Apparent equilibrium constants for Be (100), Rb (0.61 to 0.77), Sr (0.28 to 0.5), Cu (<~200) and Th (300) (Carron and Lagache, 1980; Candela and Holland, 1984; Webster et al., 1989; Bos, 1990; Candela and Piccoli, 1995; Williams et al., 1995; Simon et al., 2006) are all consistent with the K'_{BeCl_2}, K'_{RbCl}, K''_{SrCl^+}, $K'_{CuCl_2^-}$, and K'_{ThF_4} we report (Fig. 6 and Supplementary Tables 8 and 9). Apparent equilibrium constants reported for lithium range from 1 in haplogranites to 40 in fluorine-rich systems (London et al., 1989; Webster et al., 1989; Bos, 1990; Candela and Piccoli, 1995) the latter of which are considerably higher than the K'_{LiCl} we observe (maximum ~3; Fig. 6 and Supplementary Table 8). However, considering that K'_{LiCl} increases with increasing of HCl and HF, it is possible to achieve values >10 at X_{HF}^{Fluid} > 0.04. Apparent equilibrium constants for iron (Simon et al., 2004; Zajacz et al., 2008; Zajacz et al., 2012) are <~13, with Zajacz et al. (2012) reporting the lowest values in andesitic systems. These previously reported values overlap with but are slightly lower than K'_{FeCl_2} reported here (minimum of ~3; Fig. 6 and Supplementary Table 8) and this difference is likely due to the effect of the HF we observed. Similar comparisons can be made for Ca, Mg, Mn, and Zn, where literature values (Holland, 1972) are typically lower than the values we report, but the range of those values are within the range of possible apparent equilibrium constants considering the effect of HCl and HF.

Reed et al. (2000) reported apparent equilibrium constants for most REEs and Candela and Piccoli (1995) recast the data of Flynn and Burnham (1978b) for cerium and ytterbium. Reed et al. (2000) observed that apparent

equilibrium constants decreased with decreasing 8-fold ionic radius such that for Nd, $K' = 0.40$ and for Lu $K' = 0.11$. Reed et al. (2000) also noted that La and Ce do not follow this trend due to the presence of hydration shells. Likewise, Eu falls of the trend of Reed et al. (2000) probably due to its presence as both a 2+ and 3+ cation. The values for $K''_{REECl^{2+}}$ we report vary considerably with HCl and HF and the values reported by Reed et al. (2000) are within the this range. Additionally, the variation of the apparent equilibrium constant with ionic radius reported by Reed et al. (2000) is observed in the median $K''_{REECl^{2+}}$ (but less so for fluorides; Supplemental Fig. 4). There is an overall decreasing $K''_{REECl^{2+}}$ with decreasing ionic radius, as well as two distinct trends such that the $K''_{REECl^{2+}}$ decreases from La to Eu, as well as decreasing from Gd to Lu.

Our experimental results are either consistent with previously reported apparent equilibrium constants or the values can be reproduced by considering their variation with the HCl and HF content of the fluid. The only exception to this is for uranium where the previous apparent equilibrium constant is 0.4 (Keppler and Wyllie, 1991; Candela and Piccoli, 1995) and is several orders of magnitude lower than the values we report. The discrepancy in the behaviour of U is likely a result of the assumptions of our model. The speciation of uranium is restricted to either U^{3+} or UOH^{2+} due to missing chloride and fluoride species in the chosen datasets. The study of Keppler and Wyllie (1991) clearly indicate that uranium is speciated as either a fluoride or chloride species and the lack of fluoride and chloride species used in our speciation calculations is a clear limitation of this model. However, Keppler and Wyllie (1991) report partition coefficients of <0.5, which are consistent with the partition coefficients reported here. Thus, should thermodynamic data, that is consistent with the SUPCRTBL database become available, it is expected the apparent equilibrium constants for uranium chloride and fluoride species be consistent with Keppler and Wyllie (1991).

5.5. Validation of Linked Fluid and Melt Models

In order to validate the linked fluid and melt model we used the bulk composition (starting fluid + starting glass) of each experiment as input to our model and equilibrated the systems at 200 MPa and 800°C and suppressed all crystalline phases. For experiments where the starting materials were chlorine- or fluorine-free, e.g. many Bishop Tuff experiments, 0.01 wt.% of Cl and F were added to stabilize the calculation. Comparisons of experimentally measured and modelled partition coefficients are given in Fig. 12. The modelled and experimental partition coefficients fall along a 1:1 line for alkalis, transition metals, REEs, and anions. In some low-salinity experiments, there are deviations from a 1:1 line for elements such as Zn, Pb, and Fe. In the case of Zn and Pb this indicates that other Zn species are likely present. More specifically only $ZnCl_2$ or Zn^{2+} species have been considered here due to the lack of the analogous $Zn(OH)_2$ species in SUPCRTBL. In this case, systems with low chlorine concentrations are likely to underestimate the concentration of zinc, because it is not able to speciate zinc has a hydroxide. Similarly, a the lead hydroxide species $Pb(OH)_2$ has not been considered, resulting in a deviation from the 1:1 relationship. Such scenarios may lead to anomalous partition coefficients due to the underlying assumptions of the model. In the case of Fe the deviation from a 1:1 relationship maybe be due to either iron contamination of the run product fluids, and thus higher experimentally determined partition coefficients or the exclusion of other iron-bearing complexes such as ferric iron chlorides or hydrated ferrous/ferric iron species (Scholten et al., 2019). Additionally, if speciation changes for a given metal-anion pair, e.g. REE speciation from $REECl^{+2}$ to $REECl_2^+$, $REECl_3$ or $REECl_4^-$, the effect of this change will go unaccounted for and may lead to further deviation from a the 1:1 relationship.

We also compare modelled to experimental (i.e. calculated from the assumed stable species) apparent equilibrium constants for select chloride and hydroxides (Fig. 13). Similar to the partition coefficients, we find a general agreement for both chlorides and hydroxides, excluding those experiments where $\mathbf{log_{10}\, K'_i} > 5$, which again suggests missing species for those elements and thus a misfit for those species considered. It is also worth noting that for some elements such as Nd we broadly reproduce the overall behavior but poorly fit $\mathbf{K'_i}$ for chlorides and have improved, but uneven, fitting for hydroxide species. We can use the comparisons of predicted to observed behaviors to identify elements, e.g. Cu, Zn, and REEs, where additional work is required on their speciation in fluids and thermodynamic properties. These comparisons highlight the need to further explore the speciation of fluid in magmatic-hydrothermal fluids and determine if the observed relationship to HCl and HF continues or if allocation of Cl and F to other species not considered here removes this relationship and produces a single apparent equilibrium constant. Although, Fig. 12 displays a relatively restricted number of elements, similar fitting behaviors can be

expected for groups of elements (alkalis, transition metals, REEs etc.). All fitting parameters for all species and goodness of fits are provided in the supplementary information to allow for further evaluation. Overall, we are broadly able to predict the behavior of a wide array of elements, particularly where thermodynamic data for multiple species (hydroxide, chloride, and fluoride) are available or where one species is dominate.

5.6. Application and Implications

One of the primary applications of the model constructed in this work is to predict the behavior of elements in both experimental and natural magmatic-hydrothermal systems. Here we will focus on the application of this model to "unknown" experimental systems, i.e. experiments that have been conducted in P-T-X space outside of that of experiments used for model calibration, but for which partition coefficients are known. Applying this model to such systems tests its robustness and provides an example of the model's predictive power. The "unknown" experimental systems include 1) Trace element partition experiments performed by Iveson et al. (2019) and 2) the dataset of chlorine partition coefficients originally compiled by Tattitch et al. (2021) Webster and Holloway (1988), Shinohara et al. (1989), Webster (1992a), Bureau et al. (2000), Signorelli and Carroll (2000), Botcharnikov et al. (2004), Chevychelov et al. (2008), Stelling et al. (2008), Alletti et al. (2009), Webster et al. (2009), and Alletti et al. (2014), including those data from Iveson et al. (2019). The dataset of Iveson et al. (2019) was chosen as it is a self-consistent study at P-T conditions from 850 to 1050°C and pressures of 60 to 220 MPa with data available for a number of trace elements, as well as various melt compositions. Likewise, the chlorine partition coefficient database includes melt compositions from basalt to rhyolite to phonolites and fluid salinities of up to 10s of wt.% NaCl equivalent with experimental conditions ranging from temperatures of 725 to °C and pressures of 50 to 600 MPa. Given the model requires that the bulk composition of the system to be provided, i.e. starting fluid + starting glass, only experiments where the composition of the starting fluid and starting glass, as well as their relative proportions is known were included. In order to improve the stability of the MELTS and FLUIDS calculations, a small amount (0.1 or 0.001 wt.%) of FeO, MnO, MgO, and Cr_2O_3 was added to albite (Bureau et al., 2000) or haplogranite (Shinohara et al., 1989) melts. Additionally, in fluorine-free experiments 0.01 wt.% fluorine was added to the bulk compositions.

The modelled partition coefficients for trace metals are compared to reported values from Iveson et al. (2019) for K, Li, Mn, Cu, Zn, Rb, Sr, Mo, Ba, and Pb in Fig. 14A. The model is able to reproduce the reported partition coefficients for K, Li, Mn and Rb and slightly overestimates the partition coefficients for Cu and Zn. Partition coefficients for Sr and Ba are systematically overpredicted by ~1 order of magnitude. The most likely reason for this overestimation is that the thermodynamic database utilized in this study does not have data available for $SrCl_2$ or $BaCl_2$, which are suggested to be the dominate species (Iveson et al., 2019), and instead the chloride species $SrCl^+$ and $BaCl^+$ were used. Thus, the formulation of $\mathbf{K_i'}$ as presented in equation 6, may over predict the compatibility of charged species in the fluid phase. This misfit is also evident when comparing $\mathbf{K_i'}$ for Nd for both chlorides and hydroxides. Partition coefficients for Mo are unevenly reproduced, with approximately half of the values being underpredicted and half of the values falling along the 1:1 line. The partition coefficients for Pb are reproduced reasonably well, but tends to overestimate, particularly at values >1 to 2.

The modelled $\mathbf{D_{Cl}^{Fluid/Melt}}$ are compared to reported values in Fig. 14B. At a broad level the model is able to reproduce, within uncertainty, $\mathbf{D_{Cl}^{Fluid/Melt}}$ for a large range of melt compositions over a broad range of temperatures and pressures. Melt compositions including rhyolites, rhyodacites, phonolites, albite, (trachy)dacites are reproduced with the most accuracy. Basaltic melts are often underpredicted with reported $\mathbf{D_{Cl}^{Fluid/Melt}}$ ranging from 1 to 15 and modeled $\mathbf{D_{Cl}^{Fluid/Melt}}$ clustering around 1-2. Lastly, the modelled $\mathbf{D_{Cl}^{Fluid/Melt}}$ for haplogranties are systematically underpredicted by a factor of ~2.5. We also note that in select experiments from Signorelli and Carroll (2000), Webster and Holloway (1988), Chevychelov et al. (2008), and Shinohara et al. (1989) the system appears to be in a two-phase regime and a small fraction of brine is present, thus in those experiments the salinity of the vapor-and brine are fixed according to the phase relationships in the NaCl-H_2O system (Driesner, 2007; Driesner and Heinrich, 2007). The general agreement between modelled and reported $\mathbf{D_{Cl}^{Fluid/Melt}}$ is evidence of the robustness of this model to predict the behavior of chloride complexing elements. Although many of the studies in this database do not report partition coefficients for major or trace elements, i.e. Na, K, Fe, Ca, Li, Cu, Zn etc., because these elements are strongly chloride complexed, we can conclude that the their behavior can be reasonably

predicted, similar to the predictions of our model for Iveson et al. (2019) and that behavior can be determined in a wide range of P-T-X space.

In summary, the comparison of predicted vs reported partition coefficients reveals several elements/groups of elements that are easily reproduced, and others were some refinements is needed. The model presented here is most accurate for cations that are in the 1+ oxidation state, such as Na, K, Li, and Rb. Elements in higher oxidation states or those that may be present in a 2+ oxidation states are well produced, with the condition the species being considered are neutrally charged, such as Zn and Mn. In cases where thermodynamic data are not available for neutral species, and non-neutral species are considered, there is a systematic offset in predicted partition coefficients, such as for Sr and Ba. For non-neutral species where thermodynamic data is abundant, for example Cu as $CuCl_2^-$, which is a proxy for the copper species $(Na,K)CuCl_2$ (Tattitch and Blundy, 2017), the offset is less pronounced. This caveat is also likely to be the case for elements with higher oxidations states, and thus, it is evident that additional work on the speciation of highly charges elements in aqueous phases needs refinement. Further, given that many metals are strongly chloride complexed predicting the behavior of chlorine in magmatic-hydrothermal systems is now relatively straightforward. Future developments of the type of modelling presented in this work will require additional testing of species that have not been considered here due to either lack of thermodynamic or experimental data. Such testing will further refine modelling fits and accuracy of the model. Despite the limitations discussed above, at present, the linked fluid-melt model, based on the exchange of metals between an aqueous fluids and silicate melts, is able to predict the behavior of metals and chlorine in magmatic-hydrothermal systems at wide P-T-X ranges and can now be applied to a variety of systems. Such applications, have broad implications on understanding and predicting the transfer to metals in the continental crust, the degassing of volcanic systems, and formation of ore deposits.

6. Conclusions

Experiments were conducted in rhyolitic systems in order to characterize the multicomponent exchange of metals between magmatic fluids and silicate melts. The apparent equilibrium constants for the exchange of 42 major and trace elements, which are present as hydroxide, chloride, or fluoride species, were calculated by using existing thermodynamic data. We find that the apparent equilibrium constants vary as a function of the HCl and HF content of the fluid, which is a response to the acid-base neutralization of HCl by metal-hydroxide groups in the melt, as well as the incorporation of fluorine into the melt structure. By combining the experimentally determined apparent equilibrium constants, and their variation, with the MELTS family of software, crystal-melt partition coefficients, the solubility of halite and fluorite, and the behavior of NaCl, we constructed a model that is capable of calculating fluid-melt equilibria in multicomponent magmatic-hydrothermal systems. This model is capable of predicting the partitioning behavior between fluids and melt for a wide range major and trace elements in a large P-T-X space and thus can be used to constrain the evolution of fluids in magmatic-hydrothermal systems.

Acknowledgments

Austin M. Gion acknowledges funding from Agence Nationale de la Recherche through grants ANR-10-LABX-100-01 (LabEx VOLTAIRE) and ANR-11-EQPX-0036 (EquipEx PLANEX). Fabrice Gaillard acknowledges funding from Agence Nationale de la Recherche through grant ANR-18-CE31-0021 (GASTON). Nicolas Freslon, Saskia Erdmann, and Ida Di Carlo are thanked for their assistance with performing ICP-MS and IC analyses, LA-ICP-MS analyses, and EPMA analyses, respectively. The authors would also like to express their gratitude to the staff members of Expérimentation, GEOMIN, and Mesure Physique platforms, as well as the staff of IRAMAT for their support and assistance in the maintenance and operation of the laboratories and analytical facilities present at ISTO and CNRS. Paula Antoshechkin is thanked for her advice in running alphaMELTS for MATLAB. The authors are also grateful for the discussions and advice given by Michel Pichavant, Phil Piccoli, Bruno Scaillet, Mohamed Azaroual, Arnault Lassin, Andrea Carolina Ojeda-Porras, Bence Horányi and Jon Blundy. Austin M. Gion would also like to give special thanks to Philip A. Candela for his perpetual insight and willingness to discuss all aspects of thermodynamics. The authors also thank Ben Tutolo, James Brenan, Paolo Sossi, and two anonymous reviewers for their suggestions on a previous iteration of this work regarding calculations on fluid speciation.

Data Availability

Data are available through the repository Dataset for Gion and Gaillard (2025) - "The Multicomponent Exchange of Metals Between Magmatic Fluids and Silicate Melts" at https://doi.org/10.5281/zenodo.13122240. These data include experimental conditions, compositions of run products including individual point analyses for EPMA and LA-ICP-MS, results of melt and fluid speciation calculations, calculated partition coefficients and apparent equilibrium constants, as well as fits for all apparent equilibrium constants. The MATLAB code used to perform the fluid speciation calculations is available for download at https://gitlab.com/agion18/SoAP.git. This code includes the standalone applications SoAP, as well as tutorials on performing calculations are different systems. The MATLAB code for FLUIDS calculations is available at https://gitlab.com/agion18/fluids.git, including a brief tutorial on performing calculations. Citable releases of both the SoAP and FLUIDS gitlab repositories are hosted at https://doi.org/10.5281/zenodo.10365022 and https://doi.org/10.5281/zenodo.10364863, respectively.

Appendix A: Supplementary Material

The supplementary material contains additional tables and figures of the full dataset acquired as part of this work, flowcharts of modelling procedure, and BSE images of run products. Additionally, there is a supplemental discussion for justification and alternatives to the H(fasc) component, as well as additional equations describing the speciation calculations used in the present study.

Competing Interests

Fabrice Gaillard declares he an Associate Editor at Geochimica et Cosmochimica Acta.

Authors' Contributions

Conceptualization: AMG, FG

Experimentation and Modelling: AMG

Data Interpretation AMG, FG

Writing: AMG, FG

References

Alletti, M., Baker, D.R., Scaillet, B., Aiuppa, A., Moretti, R. and Ottolini, L. (2009) Chlorine partitioning between a basaltic melt and H_2O–CO_2 fluids at Mount Etna. *Chemical Geology* **263,** 37-50.

Alletti, M., Burgisser, A., Scaillet, B. and Oppenheimer, C. (2014) Chloride partitioning and solubility in hydrous phonolites from Erebus volcano: A contribution towards a multi-component degassing model. *GeoResJ* **3-4,** 27-45.

Anderson, G.M., Castet, S., Schott, J. and Mesmer, R.E. (1991) The density model for estimation of thermodynamic parameters of reactions at high temperatures and pressures. *Geochimica et Cosmochimica Acta* **55,** 1769-1779.

Antoshechkina, P.M. and Ghiorso, M.S. (2018) MELTS for MATLAB: A new Educational and Research Tool for Computational Thermodynamics, pp. ED44B-23.

Audétat, A. (2019) The Metal Content of Magmatic-Hydrothermal Fluids and Its Relationship to Mineralization Potential. *Economic Geology* **114,** 1033-1056.

Bai, T.B. and Koster van Groos, A.F. (1999) The distribution of Na, K, Rb, Sr, Al, Ge, Cu, W, Mo, La, and Ce between granitic melts and coexisting aqueous fluids. *Geochimica et Cosmochimica Acta* **63,** 1117-1131.

Bethke, C.M. (2007) *Geochemical and Biogeochemical Reaction Modeling*, 2 ed. Cambridge University Press, Cambridge.

Bodnar, R.J., Burnham, C.W. and Sterner, S.M. (1985) Synthetic fluid inclusions in natural quartz. III. Determination of phase equilibrium properties in the system H_2O-NaCl to 1000°C and 1500 bars. *Geochimica et Cosmochimica Acta* **49,** 1861-1873.

Borchert, M., Wilke, M., Schmidt, C., Cauzid, J. and Tucoulou, R. (2010a) Partitioning of Ba, La, Yb and Y between haplogranitic melts and aqueous solutions: An experimental study. *Chemical Geology* **276,** 225-240.

Borchert, M., Wilke, M., Schmidt, C. and Rickers, K. (2009) Partitioning and equilibration of Rb and Sr between silicate melts and aqueous fluids. *Chemical Geology* **259,** 39-47.

Borchert, M., Wilke, M., Schmidt, C. and Rickers, K. (2010b) Rb and Sr partitioning between haplogranitic melts and aqueous solutions. *Geochimica et Cosmochimica Acta* **74,** 1057-1076.

Borisova, A.Y., Thomas, R., Salvi, S., Candaudap, F., Lanzanova, A. and Chmeleff, J. (2012) Tin and associated metal and metalloid geochemistry by femtosecond LA-ICP-QMS microanalysis of pegmatite–leucogranite melt and fluid inclusions: new evidence for melt–melt–fluid immiscibility. *Mineralogical magazine* **76,** 91-113.

Bos, A. (1990) *Hydrothermal Element Distributions at High Temperatures: An Experimental Study on the Partitioning of Major and Trace Elements Between Phlogopite, Haplogranitic Melt and Vapour.* [PhD]:Instituut voor Aardwetenschappen Rijksuniversiteit te Utrecht, 99 p.

Botcharnikov, R.E., Behrens, H., Holtz, F., Koepke, J. and Sato, H. (2004) Sulfur and chlorine solubility in Mt. Unzen rhyodacitic melt at 850 °C and 200 MPa. *Chemical Geology* **213,** 207-225.

Botcharnikov, R.E., Holtz, F. and Behrens, H. (2015) Solubility and fluid–melt partitioning of H_2O and Cl in andesitic magmas as a function of pressure between 50 and 500 MPa. *Chemical Geology* **418**, 117-131.

Bureau, H., Keppler, H. and Métrich, N. (2000) Volcanic degassing of bromine and iodine: experimental fluid/melt partitioning data and applications to stratospheric chemistry. *Earth and Planetary Science Letters* **183**, 51-60.

Candela, P.A. (1990) Theoretical constraints on the chemistry of the magmatic aqueous phase. *Ore-bearing Granite Systems*, 11-20.

Candela, P.A. (1997) A review of shallow, ore-related granites: textures, volatiles, and ore metals. *Journal of Petrology* **38**, 1619-1633.

Candela, P.A. and Holland, H.D. (1984) The partitioning of copper and molybdenum between silicate melts and aqueous fluids. *Geochimica et Cosmochimica Acta* **48**, 373-380.

Candela, P.A. and Piccoli, P.M. (1995) Model Ore-Metal Partitioning from Melts into Vapor and Vapor/Brine Mixtures. *Magmas, fluids and ore deposits, Mineralogical Association of Canada Short Course Series* **23**, 101-127.

Candela, P.A. and Piccoli, P.M. (1998) Magmatic Contributions to Hydrothermal Ore Deposits: An Algorithm (MVPart) for Calculating the Composition of the Magmatic Volatile Phase, in: Richards, J.P., Larson, P.B. (Eds.), *Techniques in hydrothermal ore deposits geology*, Reviews in Economic Geology, pp. 97-108.

Candela, P.A. and Piccoli, P.M. (2005) Magmatic processes in the development of porphyry-type ore systems, in: Hedenquist, J.W., Thompson, J.F.H., Goldfarb, R.J., Richards, J.P. (Eds.), *Society of Economic Geologists*, pp. 25-37.

Carron, J.-P. and Lagache, M. (1980) Étude expérimentale du fractionnement des éléments Rb, Cs, Sr et Ba entre feldspaths alcalins, solutions hydrothermales et liquides silicatés dans le système Q.Ab.Or.H_2O à 2 kbar entre 700 et 800 °C. *Bulletin de Minéralogie*, 571-578.

Černý, P., Blevin, P.L., Cuney, M. and London, D. (2005) Granite-Related Ore Deposits, in: Hedenquist, J.W., Thompson, J.F.H., Goldfarb, R.J., Richards, J.P. (Eds.), *One Hundredth Anniversary Volume*. Society of Economic Geologists, pp. 337–370.

Chevychelov, V.Y., Botcharnikov, R.E. and Holtz, F. (2008) Partitioning of Cl and F between fluid and hydrous phonolitic melt of Mt. Vesuvius at ~850–1000 °C and 200 MPa. *Chemical Geology* **256**, 172-184.

Chevychelov, V.Y. and Chevychelova, T. (1998) Partitioning of Pb, Zn, W, Mo, Cl, and major elements between aqueous fluid and melt in the systems granodiorite (granite, leucogranite)-H_2O-NaCl-HCl. *Neues Jahrbuch fur Mineralogie Abhandlungen* **172**, 101-115.

Crerar, D.A. (1975) A method for computing multicomponent chemical equilibria based on equilibrium constants. *Geochimica et Cosmochimica Acta* **39**, 1375-1384.

Dingwell, D.B. and Mysen, B.O. (1985) Effects of water and fluorine on the viscosity of albite melt at high pressure: a preliminary investigation. *Earth and Planetary Science Letters* **74**, 266-274.

Dolejš, D. and Baker, D.R. (2006) Fluorite solubility in hydrous haplogranitic melts at 100 MPa. *Chemical Geology* **225**, 40-60.

Driesner, T. (2007) The system H_2O–NaCl. Part II: Correlations for molar volume, enthalpy, and isobaric heat capacity from 0 to 1000°C, 1 to 5000bar, and 0 to 1 XNaCl. *Geochimica et Cosmochimica Acta* **71**, 4902-4919.

Driesner, T. and Heinrich, C.A. (2007) The system H_2O–NaCl. Part I: Correlation formulae for phase relations in temperature–pressure–composition space from 0 to 1000°C, 0 to 5000bar, and 0 to 1 X_{NaCl}. *Geochimica et Cosmochimica Acta* **71**, 4880-4901.

Edmonds, M., Mason, E. and Hogg, O. (2022) Volcanic Outgassing of Volatile Trace Metals. *Annual Review of Earth and Planetary Sciences* **50**, 79-98.

Farnan, I., Kohn, S.C. and Dupree, R. (1987) A study of the structural role of water in hydrous silica glass using cross-polarisation magic angle spinning NMR. *Geochimica et Cosmochimica Acta* **51**, 2869-2873.

Flynn, R.T. and Burnham, C.W. (1978a) An experimental determination of rare earth partition coefficients between a chloride containing vapor phase and silicate melts. *Geochimica et Cosmochimica Acta* **42**, 685-701.

Flynn, R.T. and Burnham, W.C. (1978b) An experimental determination of rare earth partition coefficients between a chloride containing vapor phase and silicate melts. *Geochimica et Cosmochimica Acta* **42**, 685-701.

Frank, M.R., Candela, P.A. and Piccoli, P.M. (2003) Alkali exchange equilibria between a silicate melt and coexisting magmatic volatile phase: an experimental study at 800°C and 100 MPa. *Geochimica et Cosmochimica Acta* **67**, 1415-1427.

Gaillard, F., Malavergne, V., Bouhifd, M.A. and Rogerie, G. (2022) A speciation model linking the fate of carbon and hydrogen during core – magma ocean equilibration. *Earth and Planetary Science Letters* **577**, 117266.

Gammon, J.B., Borcsik, M. and Holland, H.D. (1969) Potassium-Sodium Ratios in Aqueous Solutions and Coexisting Silicate Melts. *Science* **163**, 179-181.

Ghiorso, M.S. and Gualda, G.A.R. (2015) An H_2O–CO_2 mixed fluid saturation model compatible with rhyolite-MELTS. *Contributions to Mineralogy and Petrology* **169**, 53.

Ghiorso, M.S. and Sack, R.O. (1995) Chemical mass transfer in magmatic processes IV. A revised and internally consistent thermodynamic model for the interpolation and extrapolation of liquid-solid equilibria in magmatic systems at elevated temperatures and pressures. *Contributions to Mineralogy and Petrology* **119**, 197-212.

Gion, A.M., Gaillard, F., Freslon, N., Erdmann, S. and Di Carlo, I. (2022) A method for the direct analysis of quenched, magmatic-hydrothermal fluids recovered from high-pressure, high-temperature experiments. *Chemical Geology* **609**, 121061.

Gion, A.M., Piccoli, P.M. and Candela, P.A. (2018) Partitioning of indium between ferromagnesian minerals and a silicate melt. *Chemical Geology* **500**, 30-45.

Gualda, G.A.R., Ghiorso, M.S., Lemons, R.V. and Carley, T.L. (2012) Rhyolite-MELTS: a Modified Calibration of MELTS Optimized for Silica-rich, Fluid-bearing Magmatic Systems. *Journal of Petrology* **53**, 875-890.

Guillong, M., Meier, D.L., Allan, M.M., Heinrich, C.A. and Yardley, B.W. (2008) SILLS: A MATLAB-based program for the reduction of laser ablation ICP-MS data of homogeneous materials and inclusions, in: Sylvester, P. (Ed.), *Laser Ablation ICP-MS in the Earth Sciences: Current Practices and Outstanding Issues*. Mineralogical Association of Canada Short Course 40, pp. 328-333.

Guo, H. and Audétat, A. (2017) Transfer of volatiles and metals from mafic to felsic magmas in composite magma chambers: An experimental study. *Geochimica et Cosmochimica Acta* **198**, 360-378.

Gysi, A.P., Hurtig, N.C., Pan, R., Miron, G.D. and Kulik, D.A. (2023) MINES thermodynamic database. *New Mexico Bureau of Geology and Mineral Resources, version 23*.

Hammond, G.E., Lichtner, P.C., Lu, C. and Mills, R.T. (2019) *PFLOTRAN: Reactive Flow & Transport Code for Use on Laptops to Leadership-Class Supercomputers. In: Groundwater Reactive Transport Models*. Bentham Science Publishers, United States.

Hedenquist, J.W. and Lowenstern, J.B. (1994) The role of magmas in the formation of hydrothermal ore deposits. *Nature* **370**, 519-527.

Hildreth, W. (1979) The Bishop Tuff: Evidence for the origin of compositional zonation in silicic magma chambers in: Chapin, C.E., Elston, W.E. (Eds.), *Ash-Flow Tuffs*. Geological Society of America Special Volumes.

Holland, H.D. (1972) Granites, Solutions, and Base Metal Deposits. *Economic Geology* **67**, 281-301.

Iacovino, K., Matthews, S., Wieser, P.E., Moore, G.M. and Bégué, F. (2021) VESIcal Part I: An Open-Source Thermodynamic Model Engine for Mixed Volatile (H_2O-CO_2) Solubility in Silicate Melts. *Earth and Space Science* **8**, e2020EA001584.

Iveson, A.A., Webster, J.D., Rowe, M.C. and Neill, O.K. (2019) Fluid-melt trace-element partitioning behaviour between evolved melts and aqueous fluids: Experimental constraints on the magmatic-hydrothermal transport of metals. *Chemical Geology* **516**, 18-41.

Johnson, J.W., Oelkers, E.H. and Helgeson, H.C. (1992) SUPCRT92: A software package for calculating the standard molal thermodynamic properties of minerals, gases, aqueous species, and reactions from 1 to 5000 bar and 0 to 1000°C. *Computers & Geosciences* **18**, 899-947.

Keppler, H. and Wyllie, P.J. (1991) Partitioning of Cu, Sn, Mo, W, U, and Th between melt and aqueous fluid in the systems haplogranite-H_2O–HCl and haplogranite-H_2O–HF. *Contributions to Mineralogy and Petrology* **109**, 139-150.

Kouzmanov, K., Pokrovski, G.S., Hedenquist, J.W., Harris, M. and Camus, F. (2012) Hydrothermal Controls on Metal Distribution in Porphyry Cu (-Mo-Au) Systems, *Geology and Genesis of Major Copper Deposits and Districts of the World: A Tribute to Richard H. Sillitoe*. Society of Economic Geologists, p. 0.

Kulik, D.A., Wagner, T., Dmytrieva, S.V., Kosakowski, G., Hingerl, F.F., Chudnenko, K.V. and Berner, U.R. (2013) GEM-Selektor geochemical modeling package: revised algorithm and GEMS3K numerical kernel for coupled simulation codes. *Computational Geosciences* **17**, 1-24.

Le Losq, C., Mysen, B.O. and Cody, G.D. (2015) Water and magmas: insights about the water solution mechanisms in alkali silicate melts from infrared, Raman, and 29Si solid-state NMR spectroscopies. *Progress in Earth and Planetary Science* **2**, 22.

London, D., Hervig, R.L. and Morgan, G.B. (1988) Melt-vapor solubilities and elemental partitioning in peraluminous granite-pegmatite systems: experimental results with Macusani glass at 200 MPa. *Contributions to Mineralogy and Petrology* **99**, 360-373.

London, D., Morgan, G.B. and Hervig, R.L. (1989) Vapor-undersaturated experiments with Macusani glass+H_2O at 200 MPa, and the internal differentiation of granitic pegmatites. *Contributions to Mineralogy and Petrology* **102,** 1-17.

Manning, D.A.C. and Henderson, P. (1984) The behaviour of tungsten in granitic melt-vapour systems. *Contributions to Mineralogy and Petrology* **86,** 286-293.

Mesmer, R.E., Marshall, W.L., Palmer, D.A., Simonson, J.M. and Holmes, H.F. (1988) Thermodynamics of aqueous association and ionization reactions at high temperatures and pressures. *Journal of Solution Chemistry* **17,** 699-718.

Moretti, R. and Ottonello, G. (2022) Silicate Melt Thermochemistry and the Redox State of Magmas. *Reviews in Mineralogy and Geochemistry* **87,** 339-403.

Nowak, M. and Behrens, H. (2001) Water in rhyolitic magmas: getting a grip on a slippery problem. *Earth and Planetary Science Letters* **184,** 515-522.

Papale, P., Moretti, R. and Barbato, D. (2006) The compositional dependence of the saturation surface of H_2O + CO_2 fluids in silicate melts. *Chemical Geology* **229,** 78-95.

Papale, P., Moretti, R. and Paonita, A. (2022) Thermodynamics of Multi-component Gas–Melt Equilibrium in Magmas: Theory, Models, and Applications. *Reviews in Mineralogy and Geochemistry* **87,** 431-556.

Parkhurst, D. and Appelo, C. (2013) PHREEQC (Version 3)--A Computer Program for Speciation. *Batch-Reaction, One-Dimensional Transport, and Inverse Geochemical Calculations (Denver, Colorado, USA, US Geological Survey, Water Resources Division)*.

Pichavant, M., Kontak, D.J., Briqueu, L., Herrera, J.V. and Clark, A.H. (1988) The Miocene-Pliocene Macusani Volcanics, SE Peru. *Contributions to Mineralogy and Petrology* **100,** 325-338.

Pichavant, M., Valencia Herrera, J., Boulmier, S., Briqueu, L., Joron, J.-L., Juteau, M., Marin, L., Michard, A., M.F. Sheppard, S., Treuil, M. and Vernet, M. (1987) The Macusani glasses, SE Peru: evidence of chemical fractionation in peraluminous magmas, *Magmatic Process: Physicochemical Principles.* . The Geochemical Society, pp. 359-373.

Pokrovski, G.S., Borisova, A.Y. and Bychkov, A.Y. (2013) Speciation and Transport of Metals and Metalloids in Geological Vapors. *Reviews in Mineralogy and Geochemistry* **76,** 165-218.

Reed, M.J., Candela, P.A. and Piccoli, P.M. (2000) The distribution of rare earth elements between monzogranitic melt and the aqueous volatile phase in experimental investigations at 800 °C and 200 MPa. *Contributions to Mineralogy and Petrology* **140,** 251-262.

Richards, J.P. (2011) Magmatic to hydrothermal metal fluxes in convergent and collided margins. *Ore Geology Reviews* **40,** 1-26.

Scaillet, B. and Evans, B.W. (1999) The 15 June 1991 Eruption of Mount Pinatubo. I. Phase Equilibria and Pre-eruption P–T–fO_2–fH_2O Conditions of the Dacite Magma. *Journal of Petrology* **40,** 381-411.

Scaillet, B., Pichavant, M. and Roux, J. (1995) Experimental Crystallization of Leucogranite Magmas. *Journal of Petrology* **36,** 663-705.

Scaillet, B., Pichavant, M., Roux, J., Humbert, G. and Lefevre, A. (1992) Improvements of the Shaw membrane technique for measurement and control of fH_2 at high temperatures and pressures. *American Mineralogist* **77,** 647-655.

Schaefer, B., Frischknecht, R., Guenther, D. and Dingwell, D.B. (1999) Determination of trace element partitioning between fluid and melt using LA-ICP-MS analysis of synthetic fluid inclusions in glass. *European journal of mineralogy* **11,** 415-426.

Scholten, L., Schmidt, C., Lecumberri-Sanchez, P., Newville, M., Lanzirotti, A., Sirbescu, M.-L.C. and Steele-MacInnis, M. (2019) Solubility and speciation of iron in hydrothermal fluids. *Geochimica et Cosmochimica Acta* **252,** 126-143.

Shinohara, H. (2009) A missing link between volcanic degassing and experimental studies on chloride partitioning. *Chemical Geology* **263,** 51-59.

Shinohara, H. and Fujimoto, K. (1994) Experimental study in the system albite-andalusite-quartz-NaCl-HCl-H_2O at 600°C and 400 to 2000 bars. *Geochimica et Cosmochimica Acta* **58,** 4857-4866.

Shinohara, H., Iiyama, J.T. and Matsuo, S. (1989) Partition of chlorine compounds between silicate melt and hydrothermal solutions: I. Partition of NaCl-KCl. *Geochimica et Cosmochimica Acta* **53,** 2617-2630.

Signorelli, S. and Carroll, M.R. (2000) Solubility and fluid-melt partitioning of Cl in hydrous phonolitic melts. *Geochimica et Cosmochimica Acta* **64,** 2851-2862.

Simon, A.C., Pettke, T., Candela, P.A., Piccoli, P.M. and Heinrich, C.A. (2004) Magnetite solubility and iron transport in magmatic-hydrothermal environments. *Geochimica et Cosmochimica Acta* **68,** 4905-4914.

Simon, A.C., Pettke, T., Candela, P.A., Piccoli, P.M. and Heinrich, C.A. (2006) Copper partitioning in a melt–vapor–brine–magnetite–pyrrhotite assemblage. *Geochimica et Cosmochimica Acta* **70,** 5583-5600.

Sonnenthal, E., Spycher, N., Xu, T. and Zheng, L. (2021) TOUGHREACT V4.13-OMP & TReactMech V1.0, United States.

Stelling, J., Botcharnikov, R.E., Beermann, O. and Nowak, M. (2008) Solubility of H_2O- and chlorine-bearing fluids in basaltic melt of Mount Etna at T=1050–1250 °C and P=200 MPa. *Chemical Geology* **256,** 102-110.

Stolper, E. (1982) The speciation of water in silicate melts. *Geochimica et Cosmochimica Acta* **46,** 2609-2620.

Student, J.J. and Bodnar, R.J. (1999) Synthetic Fluid Inclusions XIV: Coexisting Silicate Melt and Aqueous Fluid Inclusions in the Haplogranite–H_2O–NaCl–KCl System. *Journal of Petrology* **40,** 1509-1525.

Sublett, D.M., Gonzalez, M.M., Rimstidt, J.D. and Bodnar, R.J. (2018) Synthetic fluid inclusions XXI. Partitioning of Na and K between liquid and vapor in the H_2O-NaCl-KCl system at 600–800 °C and 500–1000 bars. *Geochimica et Cosmochimica Acta* **235,** 173-188.

Sverjensky, D.A., Harrison, B. and Azzolini, D. (2014) Water in the deep Earth: The dielectric constant and the solubilities of quartz and corundum to 60kb and 1200°C. *Geochimica et Cosmochimica Acta* **129,** 125-145.

Tang, Y. and Zhang, H. (2015) An experimental determination of W, Nb, and Ta partition coefficients between P-rich peraluminous granitic melt and coexisting aqueous fluid. *Chinese Journal of Geochemistry* **34,** 194-200.

Tattitch, B., Chelle-Michou, C., Blundy, J. and Loucks, R.R. (2021) Chemical feedbacks during magma degassing control chlorine partitioning and metal extraction in volcanic arcs. *Nature Communications* **12,** 1774.

Tattitch, B.C. and Blundy, J.D. (2017) Cu-Mo partitioning between felsic melts and saline-aqueous fluids as a function of X_{NaCleq}, f_{O2}, and f_{S2}. *American Mineralogist* **102,** 1987-2006.

Tattitch, B.C., Candela, P.A., Piccoli, P.M. and Bodnar, R.J. (2015) Copper partitioning between felsic melt and H_2O–CO_2 bearing saline fluids. *Geochimica et Cosmochimica Acta* **148,** 81-99.

Taylor, J.R., Wall, V.J. and Pownceby, M.I. (1992) The calibration and application of accurate redox sensors. *American Mineralogist* **77,** 284-295.

Thomas, R.W. and Wood, B.J. (2023) The effect of composition on chlorine solubility and behavior in silicate melts. *American Mineralogist* **108,** 814-825.

Urabe, T. (1987) The effect of pressure on the partitioning ratios of lead and zinc between vapor and rhyolite melts. *Economic Geology* **82,** 1049-1052.

Webster, J.D. (1990) Partitioning of F between H_2O and CO_2 fluids and topaz rhyolite melt. *Contributions to Mineralogy and Petrology* **104,** 424-438.

Webster, J.D. (1992a) Fluid-melt interactions involving Cl-rich granites: Experimental study from 2 to 8 kbar. *Geochimica et Cosmochimica Acta* **56,** 659-678.

Webster, J.D. (1992b) Water solubility and chlorine partitioning in Cl-rich granitic systems: Effects of melt composition at 2 kbar and 800°C. *Geochimica et Cosmochimica Acta* **56,** 679-687.

Webster, J.D. and Holloway, J.R. (1988) Experimental constraints on the partitioning of Cl between topaz rhyolite melt and H_2O and H_2O + CO_2 fluids: New implications for granitic differentiation and ore deposition. *Geochimica et Cosmochimica Acta* **52,** 2091-2105.

Webster, J.D., Holloway, J.R. and Hervig, R.L. (1989) Partitioning of lithophile trace elements between H_2O and H_2O + CO_2 fluids and topaz rhyolite melt. *Economic Geology* **84,** 116-134.

Webster, J.D., Iveson, A.A., Rowe, M.C. and Webster, P.M. (2020) Chlorine and felsic magma evolution: Modeling the behavior of an under-appreciated volatile component. *Geochimica et Cosmochimica Acta* **271,** 248-288.

Webster, J.D., Sintoni, M.F. and De Vivo, B. (2009) The partitioning behavior of Cl, S, and H_2O in aqueous vapor-±saline-liquid saturated phonolitic and trachytic melts at 200 MPa. *Chemical Geology* **263,** 19-36.

Williams, T.J., Candela, P.A. and Piccoli, P.M. (1995) The partitioning of copper between silicate melts and two-phase aqueous fluids: An experimental investigation at 1 kbar, 800° C and 0.5 kbar, 850° C. *Contributions to Mineralogy and Petrology* **121,** 388-399.

Williams, T.J., Candela, P.A. and Piccoli, P.M. (1997) Hydrogen-alkali exchange between silicate melts and two-phase aqueous mixtures: an experimental investigation. *Contributions to Mineralogy and Petrology* **128,** 114-126.

Xue, X. and Kanzaki, M. (2007) Al coordination and water speciation in hydrous aluminosilicate glasses: Direct evidence from high-resolution heteronuclear 1H–27Al correlation NMR. *Solid State Nuclear Magnetic Resonance* **31,** 10-27.

Zajacz, Z., Candela, P.A., Piccoli, P.M. and Sanchez-Valle, C. (2012) The partitioning of sulfur and chlorine between andesite melts and magmatic volatiles and the exchange coefficients of major cations. *Geochimica et Cosmochimica Acta* **89,** 81-101.

Zajacz, Z., Halter, W.E., Pettke, T. and Guillong, M. (2008) Determination of fluid/melt partition coefficients by LA-ICPMS analysis of co-existing fluid and silicate melt inclusions: Controls on element partitioning. *Geochimica et Cosmochimica Acta* **72,** 2169-2197.

Zeng, Q., Nekvasil, H. and Grey, C.P. (1999) Proton Environments in Hydrous Aluminosilicate Glasses: A 1H MAS, 1H/27Al, and 1H/23Na TRAPDOR NMR Study. *The Journal of Physical Chemistry B* **103,** 7406-7415.

Zeng, Q., Nekvasil, H. and Grey, C.P. (2000) In support of a depolymerization model for water in sodium aluminosilicate glasses: Information from NMR spectroscopy. *Geochimica et Cosmochimica Acta* **64,** 883-896.

Zhang, Y. and Ni, H. (2010) Diffusion of H, C, and O Components in Silicate Melts. *Reviews in Mineralogy and Geochemistry* **72,** 171-225.

Zhang, Y., Ni, H. and Chen, Y. (2010) Diffusion Data in Silicate Melts. *Reviews in Mineralogy and Geochemistry* **72,** 311-408.

Zimmer, K., Zhang, Y., Lu, P., Chen, Y., Zhang, G., Dalkilic, M. and Zhu, C. (2016) SUPCRTBL: A revised and extended thermodynamic dataset and software package of SUPCRT92. *Computers & Geosciences* **90,** 97-111.

Figure Captions

Fig. 1: Variation of K'_{NaCl} with density of the fluid phase with line of best fit (equation 23). Literature data are sourced from the calibration dataset of Tattitch et al. (2021), which includes data from Tattitch and Blundy (2017) and Botcharnikov et al. (2015).

Fig. 2: A) Na/K (mol) ratio and **B)** chlorine concentration of run product glass compositions plotted as a function of the molal concentration of Cl in the fluid phase.

Fig. 3: Concentration (ppm) of minor and trace elements in run product glasses plotted as a function of the molal concentration of Cl in the fluid phase.

Fig. 4: Stacked bar graph (left y-axis) of the concentration of species present as chlorides, fluorides, hydroxides, or free cations for each experimental. Inset shows low-salinity experiments with low metal loads. Note, that for a given molality of chlorine in the fluid the addition of minor amounts of fluorine results in an increase in the total metal load of the fluid. The influence of fluorine is clearly displayed by the jagged appearance of the mole fraction of metals (excluding sodium and potassium), such that Macusani-bearing experiments have higher metal loads than Bishop Tuff-bearing experiments with equivalent chlorine concentrations.

Fig. 5: Concentration (ppm) of minor and trace elements in run product fluids plotted as a function of the molal concentration of Cl in the fluid phase.

Fig. 6: Box-and-whisker plots of the apparent equilibrium constants (K'_i) for **A)** experimentally determined partition coefficients, **B**) chlorides, **C**) fluorides (right, blue axis is for NbF_5 MoF_6 and ThF_4), **D**) hydroxides, and **E**) free cations. All K'_i are calculated from the equivalent form of equation 3b for the given species and the appropriate sodium species, i.e. NaCl, NaF, NaOH, or Na+. Partition coefficients and apparent equilibrium constants for the individual REES are shown in Supplementary Fig. S4. Red dots are apparent equilibrium constants calculated from ratios of partition coefficients from the literature, see text for additional details. Black dots are outliers that are greater or less that the 25th and 75th percentiles by 1.5 times the interquartile range.

Fig. 7: Partition coefficients for lithium between fluid and melt as a function of the molal concentration of chlorine in the fluid. The data points are partition coefficients with standard deviations of the mean from the present work. Black data points are for Macusani experiments, maroon data points are experiments for fluorine-free Bishop Tuff experiments, and green data points are fluorine-bearing Bishop Tuff experiments. Regression are best fit line as described in the original studies.

Fig. 8: Variation of fluid/melt partition coefficients plotted against the duration of the experiment for A) fluorine-free Bishop Tuff experiments and B) Macusani experiments with S4 as the starting solution. Lines are moving averages of the two experiments.

Fig. 9: Comparison of measured and calculated fluid compositions. Mass balance fluid compositions were calculated as described in Gion et al. (2022).

Fig. 10: Variation of the K'_{KCl} as a function of **A**) $\log_{10} X_{HCl}^{Fluid}$ and **B**) $\log_{10} X_{HF}^{Fluid}$ and K'_{CaCl_2} as a function of **C**) $\log_{10} X_{HCl}^{Fluid}$ and **D**) $\log_{10} X_{HF}^{Fluid}$.

Fig. 11: Variation of $K'_{HCl,NaCl}$ as function of **A**) fluid/(fluid + melt) and **B**) pressure. Experiments from Williams et al. (1997) at 50 MPa were performed at 850°C, all other experiments shown were performed at 800°C. The combination of plots **A** and **B** can be fit to a surface according to equation 33a. Williams et al. (1997) and Simon et al. (2004) determined the HCl content of their experimental fluids by measuring the pH of the quenched fluid and in this work HCl is calculated as described in the supplementary files.

Fig. 12: Comparison of modelled and experimentally determined partition coefficients for each experimental run. Experiments Mac-2-S5, Mac-3-S4, Mac-5-S5, BT-1-S3, BT-3-5, BT-4-1, and BT-4-5 are not shown due to either compositional spaces that fail to equilibrate in MELTS (3 experiments) or failures to converge to a global minimum within the set number of iterations (4 experiments). Uncertainties on modelled partition coefficients is estimated to be a maximum of ~20 relative percent.

Fig. 13: Comparison of modelled and experimentally determined apparent equilibrium constants for **A)** hydroxide and **B)** chloride species. See Fig. 12 caption for additional detail on experiments shown. Uncertainties on modelled apparent equilibrium constants is estimated to be a maximum of ~20 relative percent.

Fig. 14: A) Comparison of modelled and previously reported fluid/melt partition coefficients for trace elements and chlorine. Previously report partition coefficients are taken from Iveson et al. (2019). **B)** Modelled and previously reported Cl fluid/melt partition coefficients. See text for literature sources. Red outline for data points indicates a poor fit for parameters 1 through 4 described in the section 4.4. Uncertainties on modelled apparent equilibrium constants is estimated to be a maximum of ~20 relative percent.

Table 1: Composition of Starting Glasses

wt%	Bishop Tuff (n=10)	Macusani (n=9)
SiO_2	76.1(2)	72.4(2)
Al_2O_3	12.5(1)	15.9(1)
TiO_2	0.06159(3)	0.03477(4)
FeO	0.65(4)	0.55(5)
MnO	0.0321(3)	0.054(5)
MgO	0.1	b.d.
CaO	0.47(1)	0.20(1)
Na_2O	3.61(4)	4.17(3)
K_2O	5.11(4)	3.79(4)
Li_2O	0.01	0.69
B_2O_3	0.02	0.57
P_2O_5	b.d.	0.55(2)
F	b.d.	1.23(2)
Cl	b.d.	0.065(4)
-O = F,Cl	0	0.5
Total	98.7(2)	99.7(2)

ASI	1			1.49	
ppm	Bishop Tuff (n=5)	Macusani (n=5)		Bishop Tuff (n=5)	Macusani (n=5)
Be	4.3(1)	37.584(3)	La	25(5)	0.80(1)
Sc	3.48(3)	3.07(1)	Ce	48(5)	1.872(2)
V	0.33(1)	0.05(4)	Pr	5.6(8)	0.23(1)
Cr	0.78(3)	0.3(1)	Nd	19(2)	0.86(2)
Co	35.2(4)	0.03(7)	Sm	4.0(2)	0.39(3)
Ni	2.0(3)	b.d.	Eu	0.041(1)	0.01(8)
Cu	5.4(1)	1.40(1)	Gd	3.5(1)	0.42(3)
Zn	27.8(3)	86.11(1)	Tb	0.54(1)	0.10(2)
Ga	14.9(1)	33.77(1)	Dy	3.61(4)	0.55(2)
Ge	1.78(4)	4.65(2)	Ho	0.72(1)	0.09(2)
Rb	174.5(7)	1,127.954(4)	Er	2.22(2)	0.23(1)
Sr	5.6(1)	1.05(1)	Tm	0.325(4)	0.04(5)
Y	21.1(2)	2.797(4)	Yb	2.35(3)	0.24(3)
Nb	21.5(2)	43.208(5)	Lu	0.34(1)	0.03(6)
Mo	6.4(1)	0.2(1)	Ta	2.48(2)	21.10(1)
Cd	0.07(1)	0.09(4)	W	375(9)	69.99(1)

In	0.0228(4)	0.888(9)	Au	0.011(1)	0.01
Sn	2.66(2)	193.83(1)	Pb	27.3(2)	8.92(1)
Cs	5.12(2)	519.098(3)	Th	19.3(3)	0.94(1)
Ba	8.0(1)	1.05(2)	U	6.8(1)	18.74(1)

Composition of staring Bishop Tuff and Macusani glass starting materials. The composition of the starting glasses are given in wt% for major element and ppm for trace elements. Uncertainty in the last digit(s) reported is given in parentheticals. N equals number of analyses. Major elements determined by EPMA and trace elements, including Li_2O and B_2O_3, were determined by LA-ICP-MS.

Table 2: Composition of Starting Solutions

M	S1	S2	S3	S4	S5
NaCl	0	0	0	0.25	1
KCl	0	0	0	0.25	1
HCl	0	0.0001	0.1	0.0001	0.0001

The compositions of the aqueous solutions are given in molar (M).

Table 3: Experimental run conditions

Run Group and Run Solution[a]		Starting Glass (mg)	Starting Fluid (mg)	Starting Quartz (mg)	Melt[b] (mg)	Supercritical Fluid[b] (mg)	Fluorine Mixture + Amorphous Silica[c] (mg)	Pressure (MPa)	Temperature (°C)	Duration (hours)[d]	Oxygen Fugacity (ΔQFM)[e]	Total Wt Difference (mg)[f]
Mac-2	S2	49.5	50.2	40.3	53.7	47.7	-	196	800	116	0.12(1)	0.2

	S3	50	50.2	39	53.4	47.8	-					0.2
	S4	50.7	51.4	30.1	54.8	49.1	-					0.3
	S5	50.9	54	35.6	55.2	50.9	-					0.3
Mac-3	S1	49.9	50.4	37.6	49.7	51.9	-	201	800	166.5	-0.31(3)	0.3
	S2	50.2	50.6	40.8	55.4	48.9	-					0.2
	S3	51.3	51.6	35.1	54.2	51.1	-					0.2
	S4	50.3	49.7	29.2	53.1	48.3	-					0.2
Mac-4	S4-3	26.4	5	42.5	n/a	4.1	-	198	800	141.5	0.08(2)	0.9
Mac-5	S2	47.8	24.2	41	52.1	21.4	-	192	800	141	0.024(5)	0.2
	S3	47.3	24.4	52.8	51.7	21.4	-					0.2
	S5	48.4	26.2	21.7	53.8	22.5	-					0
Mac-6[g]	S4	18.9	10	27.3	14.9	12.7	-	200	800	450	Vessel	0.5
Mac-7[g]	S4	19.8	10.2	26.3	21.5	9.3	-	200	800	644	Vessel	0
Mac-8*[g]	S4	50.1	50.3	11.5	52.3	48.5	-	200	800	163 +1	0.090(8)	0.4
BT-1	S1	24.4	24.6	35.9	26.6	24.4	-	192	800	142.75	-0.354(4)	0.2
	S2	24.7	25.1	27.1	31.9	25.1	-					0.2
	S3	24.6	25.1	27.1	23.2	24.8	-					0.1
	S4	25.4	25.4	29.4	26.8	25.8	-					0.1
	S5	24.6	27.2	26.9	24.6	27.4	-					0

BT-2	S1	48.6	25.3	18.8	50.8	23.7	-	198	800	141.75	-0.376(5)	0
	S2	49.2	25.1	27.9	50.3	25.9	-					0.3
	S3	48.8	25.5	32.9	53.6	23.7	-					0.2
	S4	48.9	23.9	26	49.4	22.8	-					0.4
	S5	52.4	26.7	35.3	52.5	25.6	-					0.3
BT-3	S4-5	24.3	26.1	31.6	29.1	28	1.7 + 4.4	198	800	237.5	0.6(1)	0.5
BT-4	S4-1	39.8	20.8	37.2	41	19.8		191.6	800	263	0.418(8)	0.3
	S4-2	39.7	26	31.2	43.7	25.2	1.4 + 1.5					0.4
	S4-4	40.5	21.1	4.8	24.3	19.5	1.2 + 4.8					0.1
	S4-5	39.8	20.7	25.9	51.1	19.3	1.7 + 6.5					0.3
BT-5[g]	S4	21	10.2	38.6	21.5	9.1	-	200	800	450	Vessel	0.5
BT-6[g]	S4	31.8	10.3	31.8	29.5	9.6	-	200	800	644	Vessel	0.3
BT-7*[g]	S4	51.4	50.6	28.7	55.3	49.1	-	200	800	163 +1	0.090(8)	0.1

[a]Run Group refers to the experimental run and Run Solution refers to the solution (Table 2) added to the experiment. Mac refers to experiments performed with the Macusani starting glass and BT refers to experiments performed with the Bishop Tuff Starting Glass. For example, the Mac-2 group has five capsules each with a different solution (S1-S5) and those 5 capsules were loaded into the IHPV at the simultaneously. Additional numbers included in the run solution (e.g. "-1" in "S4-1") indicate replicates of each solution.

[b]Melt and Supercritical Fluid refer to the mass of the melt and supercritical fluid phase present during the experiment at the temperature and pressure of the run.

[c]Fluorine Mixture refers to the mass of NaF:KF:AlF3 mixture added the experiment.

[d]The duration of experiment BT-7-S4/Mac-8-S4 include one additional hour before drop quench.

[e]The digit in parenthetical is the uncertainty in the last digit in measured oxygen fugacity by CoPd sensors. Oxygen fugacities marked "Vessel" are buffered by the cold-seal pressure vessel and are ~NNO.

[f]The Total Wt Difference is the absolute value of the difference between the total weight of the capsule before and after the run, experiments with differences greater than 1 mg were rejected. n/a indicates not available.

[g]Additionally, pairs of experiments Bt-6-S4/Mac-7-S4, BT-5-S4/Mac-6-S4, and BT-7-S4/Mac-8-S4 were performed simultaneously in cold-seal pressure vessels.

*Indicates drop quench experiments

Table 4: Species considered in Speciation Modelling

Chlorides	Fluorides	Hydroxides	Free Cations/Anions
LiCl	-	LiOH	Li^{1+}
$BeCl_2$	BeF_2	-	Be^{2+}
NaCl	NaF	NaOH	Na^{1+}
-	AlF_3	$AlOH_3$	Al^{3+}
KCl	-	KOH	K^{1+}
$CaCl_2$	-	-	Ca^{2+}
-	-	$ScOH^{2+}$	Sc^{3+}
-	CoF^{+}	VOH^{2+}	V^{3+}
$FeCl_2$	FeF^{+}	$FeOH^{+}$	Fe^{2+}
$CoCl^{+}$	-	$CoOH^{+}$	Co^{2+}
$NiCl^{+}$	NIF^{+}	$NiOH^{+}$	Ni^{2+}

$CuCl_2^-$	-	$CuOH_2^-$	Cu^{1+}
$ZnCl_2$	-	-	Zn^{2+}
-	-	$GaOH^{2+}$	Ga^{3+}
RbCl	RbF	RbOH	Rb^{1+}
$SrCl^+$	SrF^+	$SrOH^+$	Sr^{2+}
-	-	YOH^{2+}	Y^{3+}
$CdCl_2$	CdF_2	-	Cd^{2+}
$BaCl^+$	BaF^+	$BaOH^+$	Ba^{2+}
$PbCl_2$	PbF_2	-	Pb^{2+}
-	-	UOH^{2+}	U^{3+}
$LaCl^{2+}$	LaF^{2+}	$LaOH^{2+}$	La^{3+}
$CeCl^{2+}$	CeF^{2+}	$CeOH^{2+}$	Ce^{3+}
$PrCl^{2+}$	PrF^{2+}	$PrOH^{2+}$	Pr^{3+}
$NdCl^{2+}$	NdF^{2+}	$NdOH^{2+}$	Nd^{3+}
$SmCl^{2+}$	SmF^{2+}	$SmOH^{2+}$	Sm^{3+}
$EuCl^{2+}$	EuF^{2+}	$EuOH^{2+}$	Eu^{3+}
$GdCl^{2+}$	GdF^{2+}	$GdOH^{2+}$	Gd^{3+}
$TbCl^{2+}$	TbF^{2+}	$TbOH^{2+}$	Tb^{3+}

$DyCl^{2+}$	DyF^{2+}	$DyOH^{2+}$	Dy^{3+}
$HoCl^{2+}$	HoF^{2+}	$HoOH^{2+}$	Ho^{3+}
$ErCl^{2+}$	ErF^{2+}	$ErOH^{2+}$	Er^{3+}
$TmCl^{2+}$	TmF^{2+}	$TmOH^{2+}$	Tm^{3+}
$YbCl^{2+}$	YbF^{2+}	$YbOH^{2+}$	Yb^{3+}
$LuCl^{2+}$	LuF^{2+}	$LuOH^{2+}$	Lu^{3+}
$MgCl_2$	-	-	-
$MnCl_2$	-	-	-
CrClOH	-	-	-
-	NbF_5	-	-
-	MoF_6	-	-
-	ThF_4	-	-
-	-	BOH_3	-
HCl	HF	H_2O	H^+
-	-	-	Cl^-
-	-	-	OH^-
-	-	-	F^-

Declaration of interests

☐ The authors declare that they have no known competing financial interests or personal relationships that could have appeared to influence the work reported in this paper.

☒ The author Fabrice Gaillard is an Associate Editor for *Geochemica et Cosmochimica Acta* and was not involved in the editorial review or the decision to publish this article.

☐ The authors declare the following financial interests/personal relationships which may be considered as potential competing interests:

Figure 1

Click here to access/download;Figu

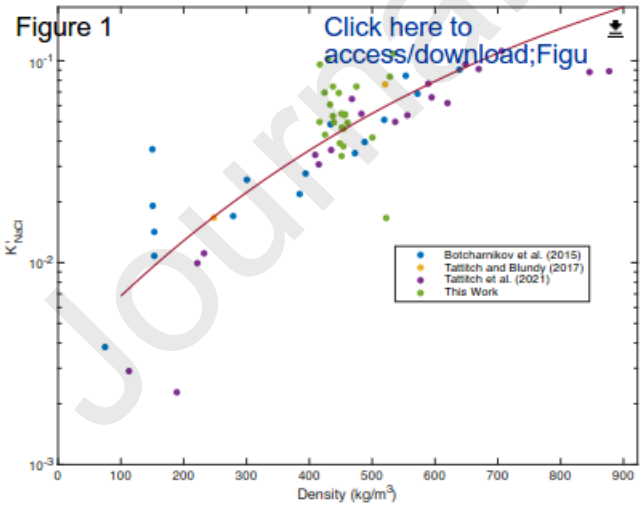

Figure 2

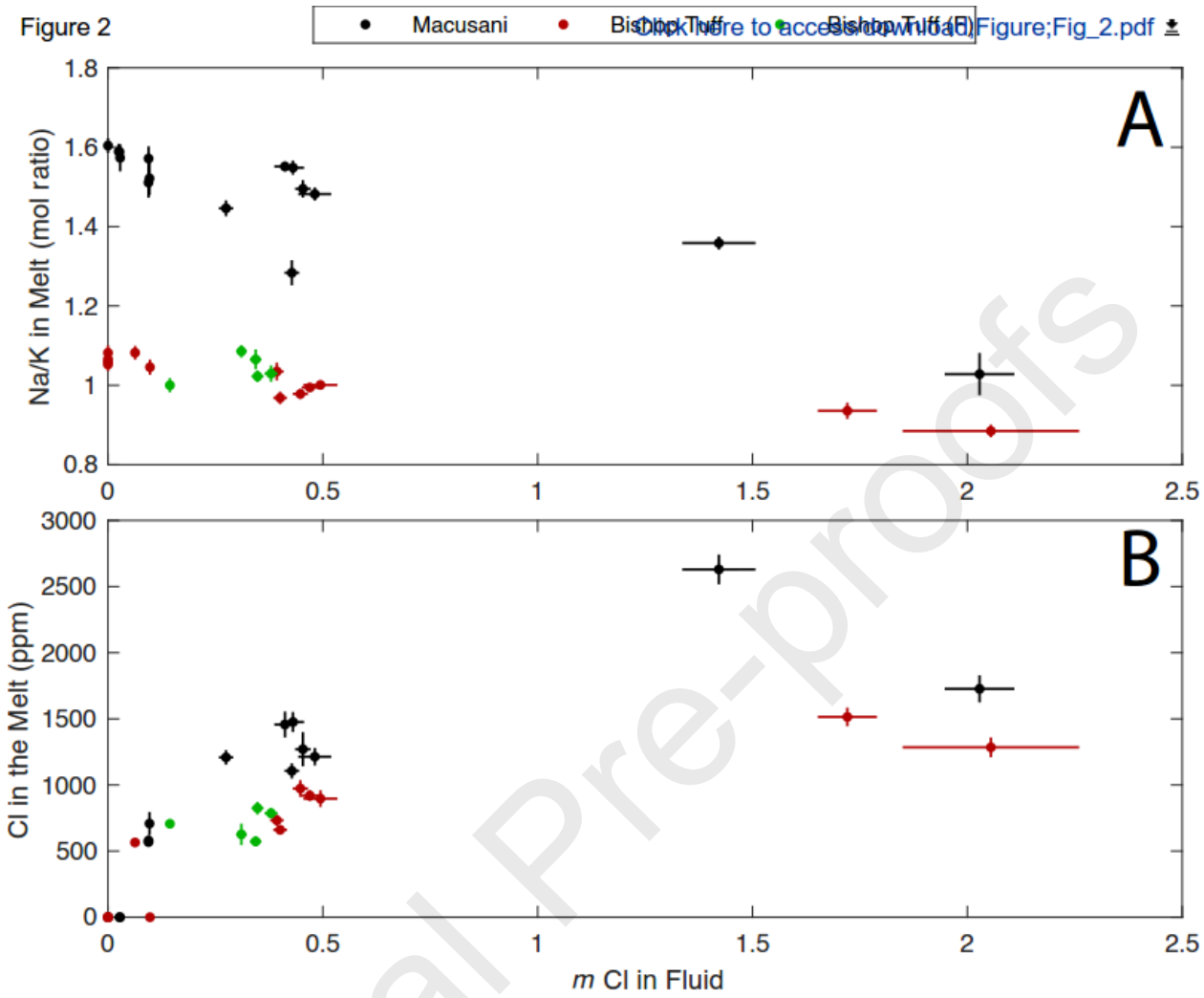

Figure 3

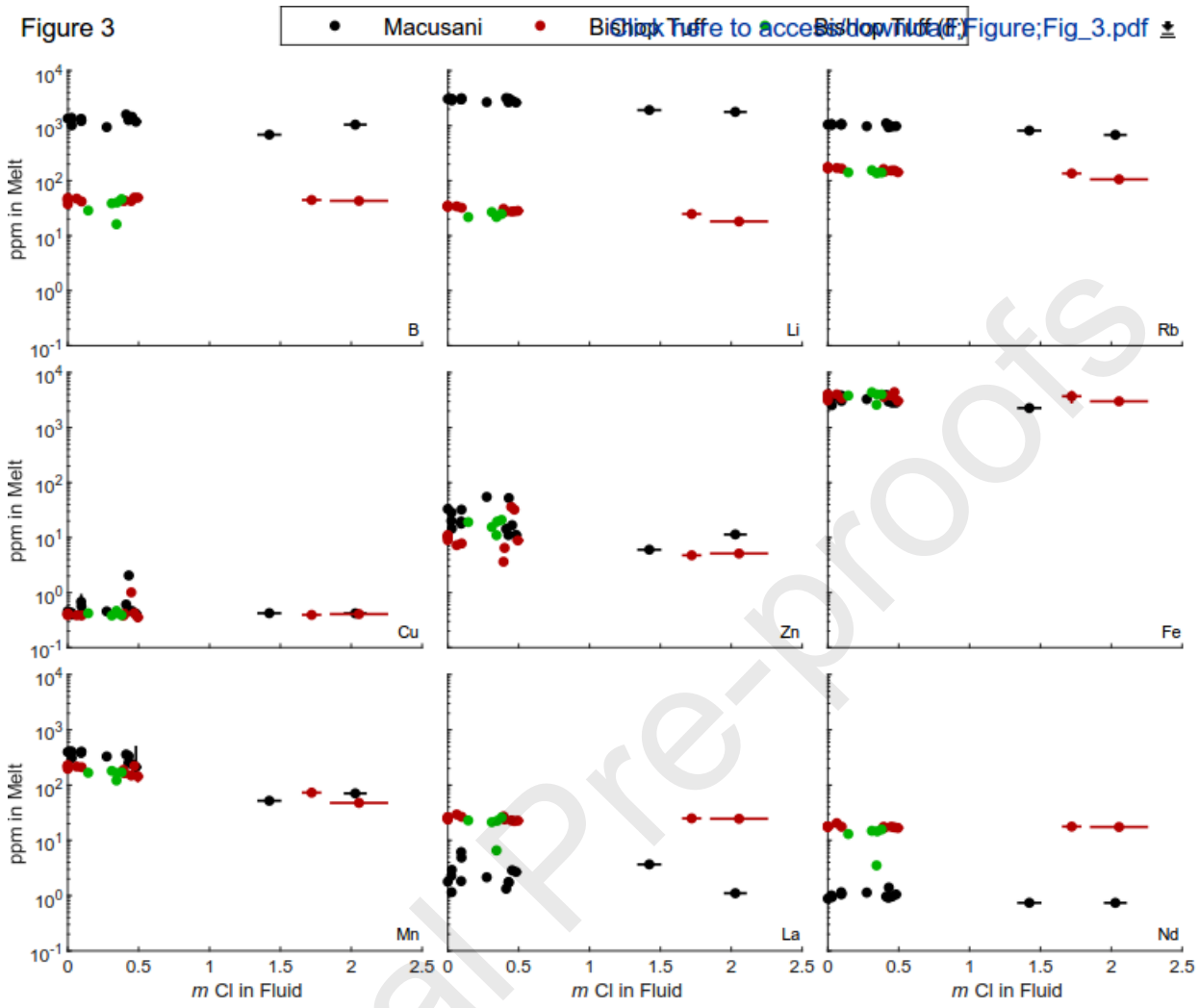

Figure 4

Click here to access/download;Figure;Fig_4.pdf

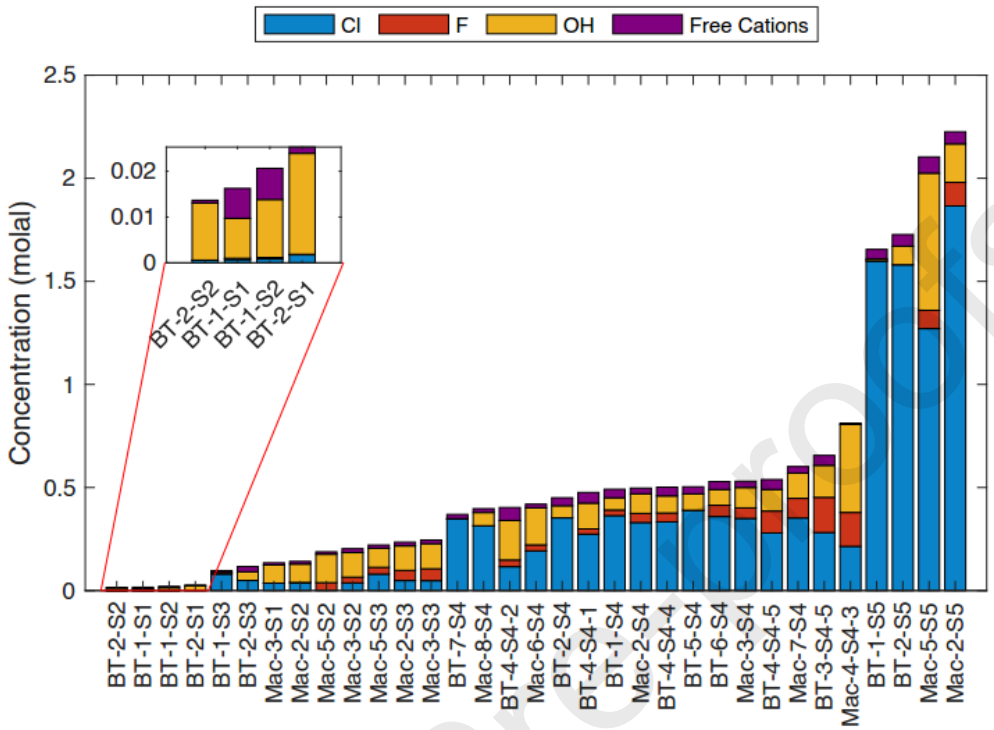

Figure 5

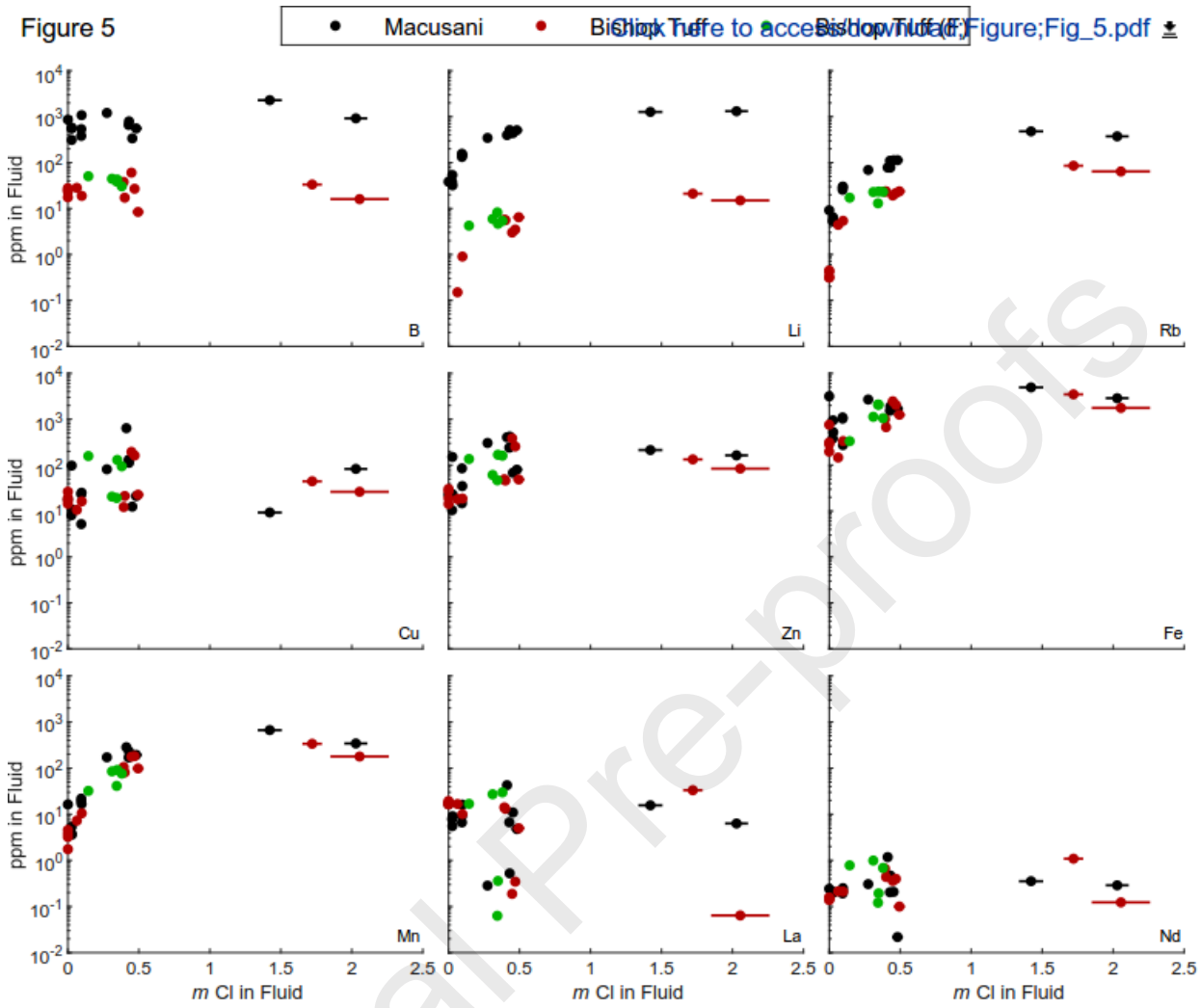

Figure 6

Click here to access/download;Figu

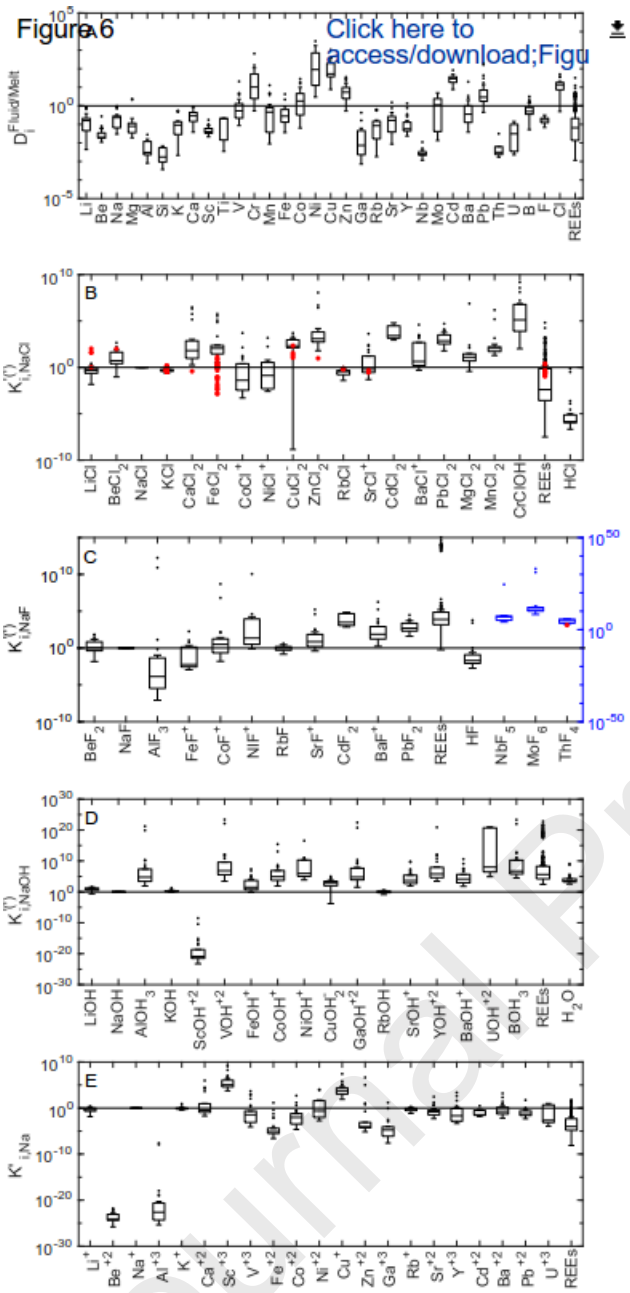

Figure 7

Click here to access/download;Fi

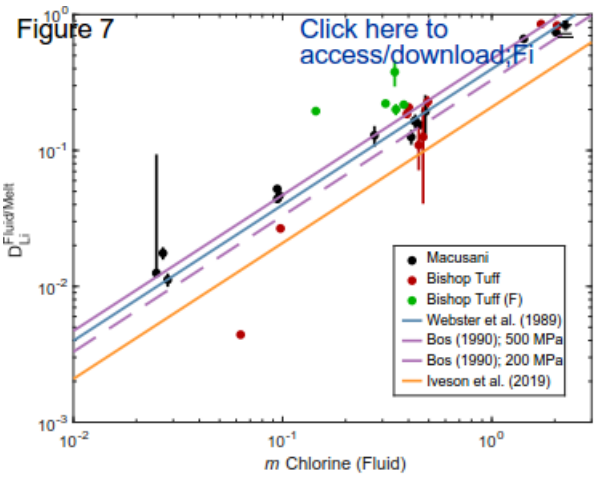

Figure 8

Click here to access/download;Figure;Fig_8.pdf

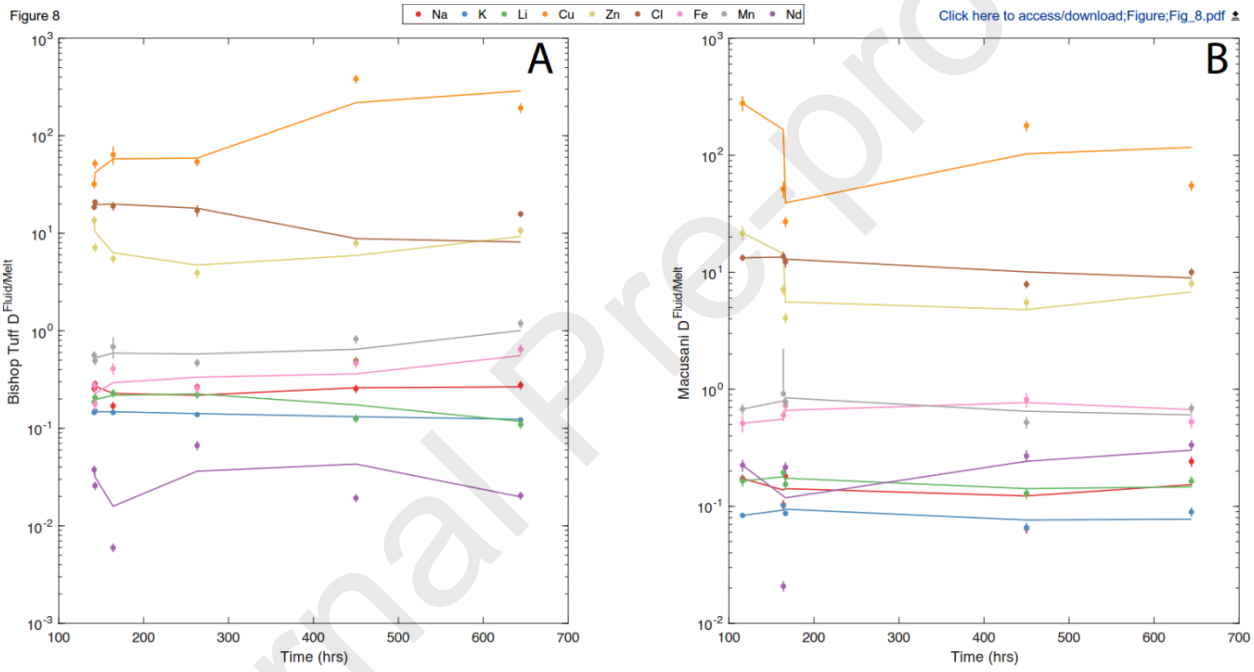

Figure 9

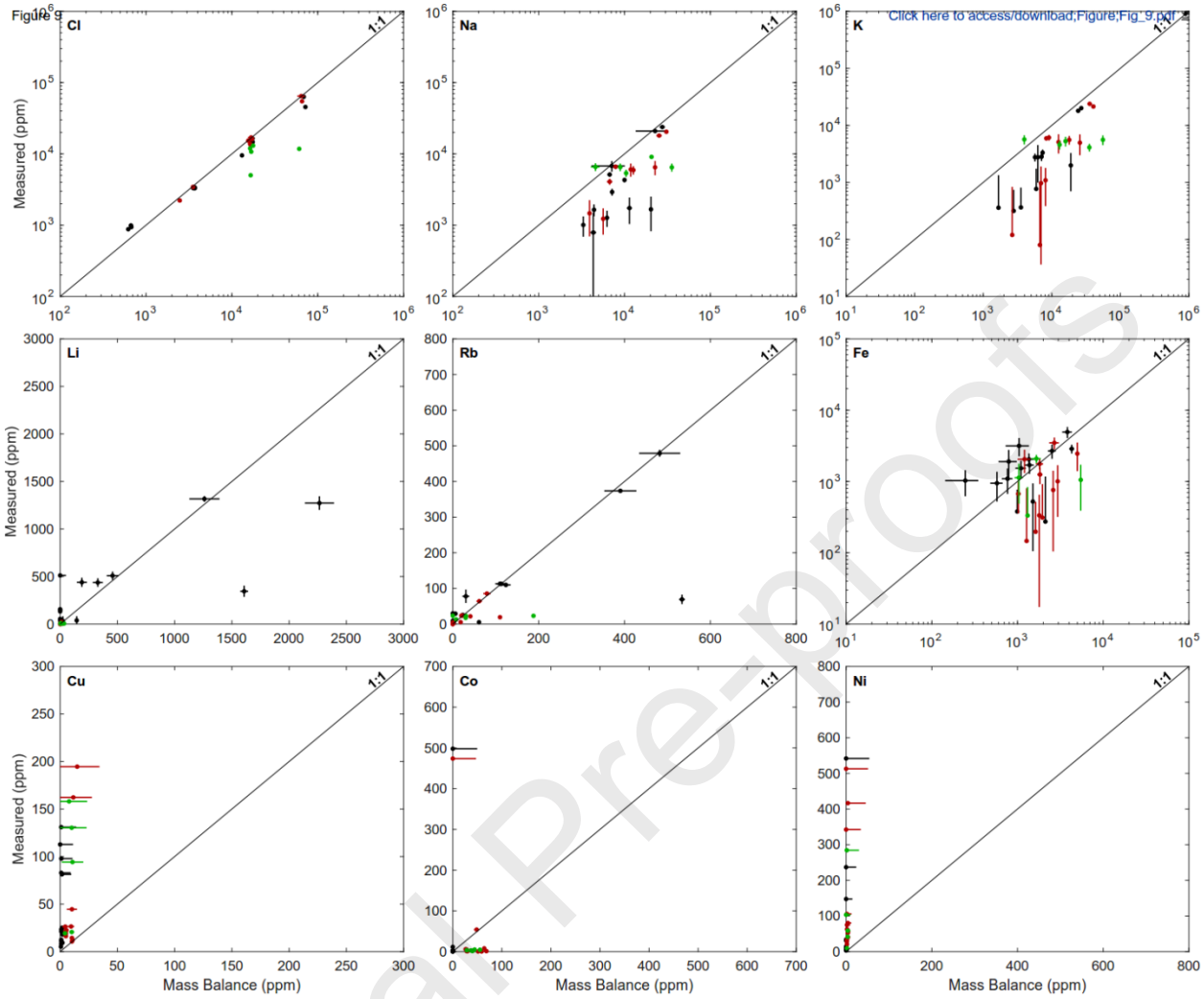

Figure 10

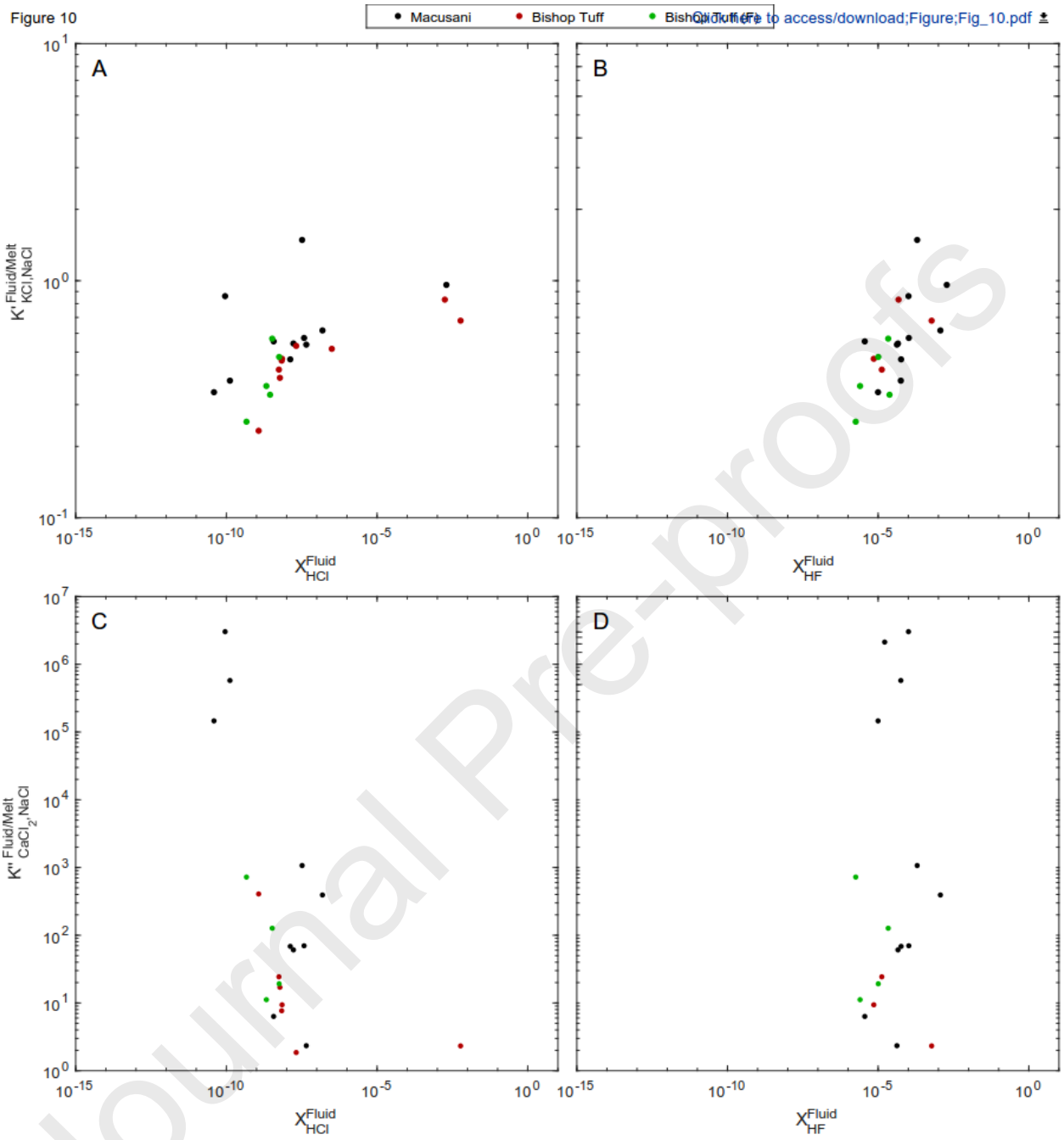

Figure 11

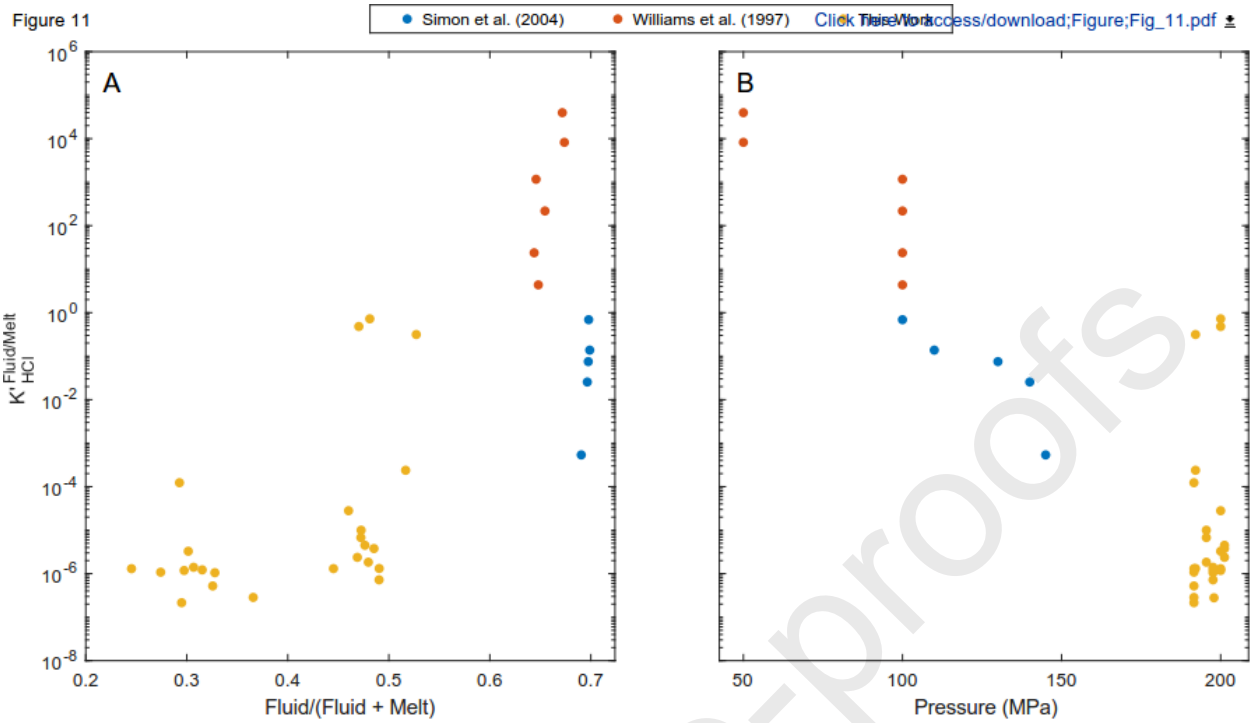

Figure 12

Click here to access/download;Figure;Fig_12.pdf

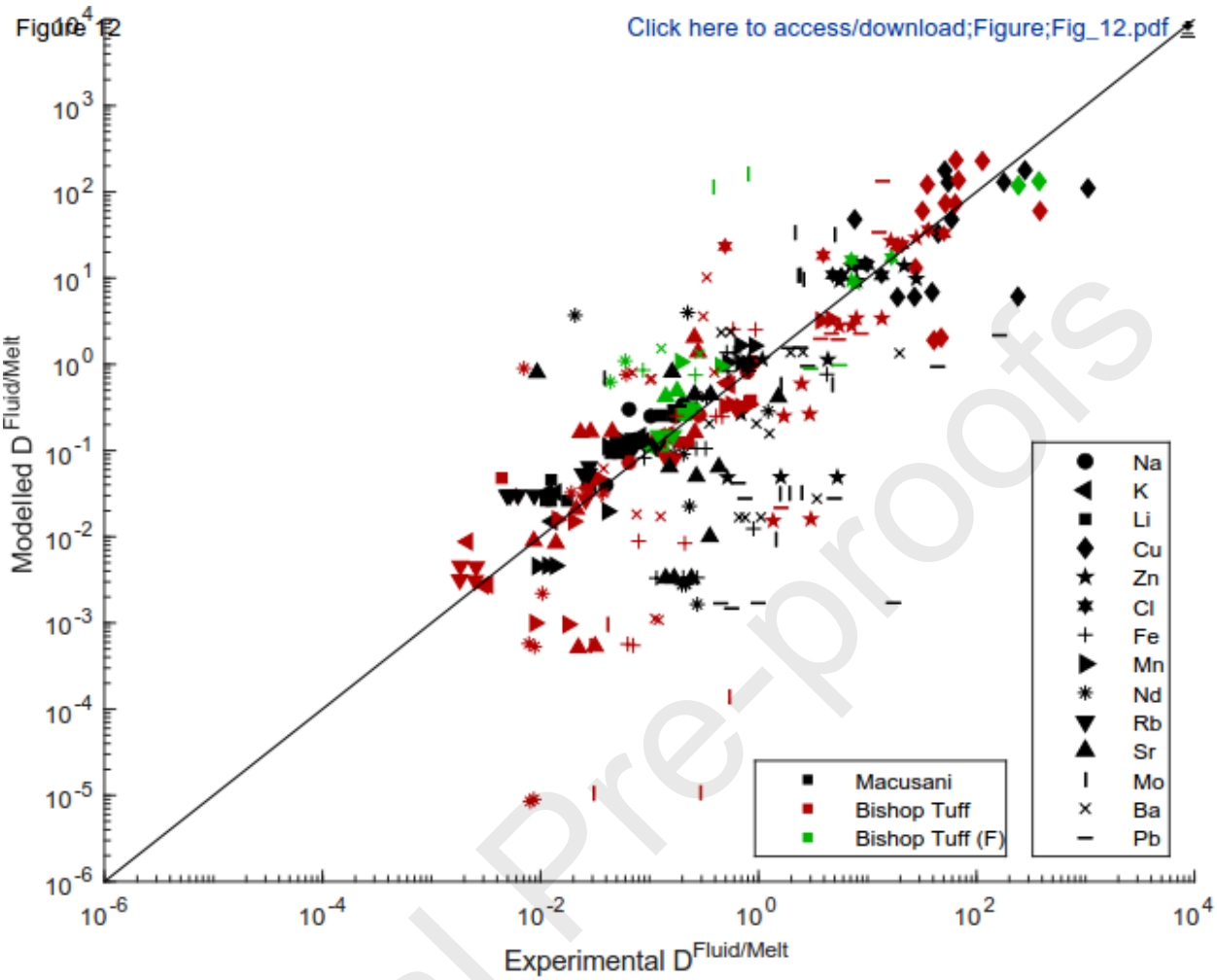

Figure 13

Click here to access/download;Figure;Fig_13.pdf